

Low Mass Stars and Brown Dwarfs in Praesepe

D.E.A. Baker^{1*}, R.F. Jameson¹, S.L. Casewell¹, N. Deacon^{2,3}, N.Lodieu^{4,5} and N. Hambly⁶

^[1] *Department of Physics and Astronomy, University of Leicester, University Road, Leicester, LE1 7RH, U.K.*

^[2] *Department of Astrophysics, Faculty of Science, Radboud University Nijmegen, PO Box 9010, 6500 GL Nijmegen, The Netherlands*

^[3] *Institute for Astronomy, University of Hawaii, 2680 Woodlawn Drive, 96822, Honolulu, Hawaii, USA*

^[4] *Instituto de Astrofísica de Canarias, C/ vía Láctea s/n, E-38200 La Laguna, Tenerife, Spain*

^[5] *Departamento de Astrofísica, Universidad de La Laguna, E-38250 La Laguna, Tenerife, Spain*

^[6] *Institute for Astronomy, SUPA (Scottish Universities Physics Alliance), University of Edinburgh, Royal Observatory, Blackford Hill, Edinburgh, EH9 3HJ, U.K.*

30th June 2010

ABSTRACT

Presented are the results of a large and deep optical-near-infrared multi-epoch survey of the Praesepe open star cluster using data from the UKIDSS Galactic Clusters Survey. Multiple colour magnitude diagrams were used to select potential members and proper motions were used to assign levels of membership probability. From our sample, 145 objects were designated as high probability members ($p \geq 0.6$) with most of these having been found by previous surveys although 14 new cluster members are also identified. Our membership assignment is restricted to the bright sample of objects ($Z < 18$). From the fainter sample, 39 candidates were found from an examination of multiple colour magnitude plots. Of these, 2 have small but significant membership probabilities. Finally, using theoretical models, cluster luminosity and mass functions were plotted with the later being fitted with a power law of $\alpha = 1.11 \pm 0.37$ for the mass range 0.6 to 0.125 M_{\odot} and an assumed cluster age of 500 Myrs in the UKIDSS Z photometric band. Likewise taking an assumed cluster age of 1 Gyr we find $\alpha = 1.10 \pm 0.37$. Similar values were also found for the J and K bands. These results compare favourably with the result of Kraus & Hillenbrand (2007) ($\alpha = 1.4 \pm 0.2$) but are significantly lower than that of the more recent study conducted by Boudreault et al. (2009) ($\alpha = 1.8 \pm 0.1$).

Key words: stars: low-mass, brown dwarfs, luminosity function, mass function - Galaxy: open clusters and associations:individual: Praesepe

1 INTRODUCTION

Low mass stars (LMS) and Brown Dwarfs (BDs) are the lowest mass objects for which the stellar formation process is applicable (Burrows et al. 2001). Locating these objects in a cluster is particularly important as it provides some of the key parameters that help define them, notably age, distance and metallicity. These can in turn be used to help provide constraints to theoretical evolutionary and atmospheric models. Another important reason for trying to locate these objects in clusters, particularly older ones, is that as the cluster ages it undergoes a process of dynamical evolution, in which the lower mass objects are preferentially ejected from the cluster into the field (de La Fuente Marcos & de La Fuente Marcos 2000). This

ejection of objects causes changes to occur in the cluster's luminosity and mass function, which for a gravitationally bound association can be considered a proxy for the initial mass function (IMF) of the system. Although there have been many previous studies aimed at characterising the IMF, they have often come from many surveys conducted in different filters and with different instruments. For this reason the UKIDSS Galactic Clusters Survey (GCS; Lawrence et al. 2007) was devised. One of the clusters surveyed is the open star cluster of Praesepe.

Praesepe lies at a distance of ≈ 180 pc ($(M - m)_0 = 6.30 \pm 0.003$, van Leeuwen 2009) with zero reddening and near solar metallicity. Whilst the distance is fairly well constrained, there is a lack of agreement with regards to its age. Allen (1973) placed the value of Praesepe's age towards the lower end of the scale at 430 Myr and it was the standard value for many years. Later work by Vandenberg & Bridges

* E-mail: deab1@star.le.ac.uk

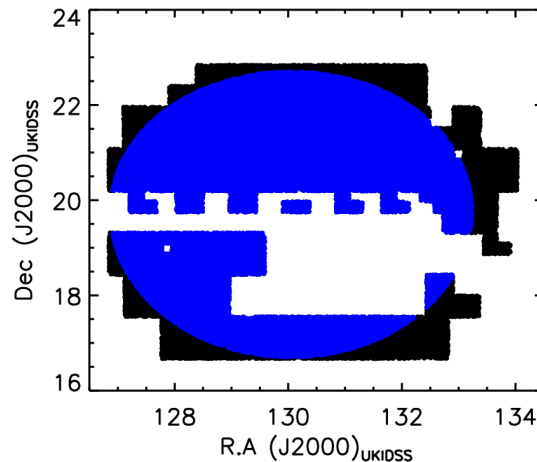


Figure 1. The full coverage of the Praesepe star cluster available from UKIDSS DR6 with the blue region denoting the sources present in the 3 degree radial selection.

(1984) placed it at a much higher value of 900 Myr. Their value was obtained via the fitting of models describing the main-sequence to the observed colour magnitude diagrams (CMDs). The widest range of age estimates is reported by Tsvetkov (1993) who placed a similar lower limit of 540 Myr but an upper limit of over 1.5 Gyrs. The method of Tsvetkov does not depend on the fitting of the Zero-Age-Main-Sequence but instead relied on models used to calculate the ages of δ Scuti stars that are present within the cluster. Finally, Kharchenko et al. (2005) placed the age in the middle at 795 Myrs after using the Padova grid of post main sequence isochrones from Girardi et al. (2002). We consider this to be closest to the most likely age as there is some evidence that the Hyades cluster at 625 Myrs shares a common origin with Praesepe (Eggen 1960; Henry et al. 1977). However due to the uncertainty that exists, two ages for the cluster have been adopted throughout this paper. The first is an age of 500 Myr and the second 1 Gyr. These were chosen as they coincide nicely with ages for which the NextGen (Baraffe et al. 1998) and DUSTY (Chabrier et al. 2000) theoretical models have been calculated. In this work we have used the BT-NextGen and BT-DUSTY models which are based on the aforementioned versions except they have been calculated with updated opacity data¹.

Praesepe’s members all have a common proper motion centred around $\mu_\alpha = -35.81 \text{ mas yr}^{-1}$ and $\mu_\delta = -12.85 \text{ mas yr}^{-1}$, again from the work by van Leeuwen based on re-reduced Hipparcos data. This distinct proper motion allows relatively easy photometric and astrometric membership surveys to take place. The “high-mass” stellar population ($V < 13$) was identified by Klein-Wassink (1927) with “intermediate-mass” ($V < 17$) and “low-mass” M-dwarfs ($R > 20$) being identified by Jones & Cudworth (1983) and Hambly et al. (1995a) respectively. Further work has been carried out by Pinfield et al. (1997, 2003), Adams et al. (2002), Chappelle et al. (2005) and González-García et al. (2006). However, these surveys have often proved to be

contaminated with an excess of field stars, as in the case of Adams et al. or have no proper motion information (Pinfield et al. 1997). The most comprehensive study to date was produced by Kraus & Hillenbrand (2007), who used data from the Sloan Digital Sky Survey (SDSS; York et al. 2000), Two Micron All Sky Survey (2MASS; Skrutskie et al. 2006), USNOB1.0 (Monet et al. 2003) and finally UCAC2 (Zacharias et al. 2004) to find 1010 candidate members of Praesepe, 442 being identified for the first time, down to a spectral type of around M5. The work presented in this paper is again a return to a search for this “low-mass” population, however we have based our search on data made available from the UKIRT Infrared Deep Sky Survey (UKIDSS), 2MASS and SDSS.

2 THE SURVEYS

UKIDSS is a near-infrared sky survey that aims to survey some 7500 square degrees of the northern sky within its science operation lifetime. The depth that it aims to achieve will be three magnitudes deeper than that offered by 2MASS, making UKIDSS an ideal companion to the SDSS in areas where the two coincide. UKIDSS uses the United Kingdom Infrared 3.8m Telescope (UKIRT) located on Mauna Kea and the Wide Field CAMera (WFCAM). WFCAM itself consists of four Rockwell Hawaii-II (HgCdTe) detectors, each of dimension 2048 x 2048 pixels. A single pixel represents a scale of 0.4 arc seconds and the spacing between the detectors requires that four paw-prints be undertaken in order to construct a single 0.8deg^2 tile. The UKIDSS survey program consists of five separate components. The Large Area Survey, The Galactic Plane Survey, The Deep Extragalactic Survey, The Ultra Deep Survey and The Galactic Clusters Survey, which provides the focus and data for this paper. For more specific information on the UKIDSS programme a set of reference papers have been produced which aim to provide technical documentation on the infrared survey instrument itself (WF-

¹ <http://phoenix.ens-lyon.fr/simulator/index.faces>

CAM; Casali et al. 2007), the WFCAM photometric system (Hewett et al. 2006; Hodgkin et al. 2009), the UKIDSS surveys (Lawrence et al. 2007), the pipeline processing system (Irwin et al. in preparation) and finally the science archive as described in Hambly et al. (2008).

The GCS aims to enable a comprehensive study of 10 star-forming regions and clusters, with hopes of detailing the form of the IMF and how it is affected by the environment in the sub-stellar regime. All the data for these programmes is processed by the Cambridge Astronomical Survey Unit (CASU) and then archived and released by the WFCAM Science Archive (WSA) located in Edinburgh. Currently, UKIDSS is on data release 6 (DR6) as of 13th October 2009 for the ESO community (and DR3 as of the 5th June 2009 for the world release). DR6 has reported depths of $Z = 20.4$, $Y = 20.1$, $J = 19.6$, $H = 18.8$ and $K = 18.2$ (first epoch). At the time of writing the Praesepe cluster has not yet been fully surveyed with only ≈ 23 square degrees being available in all filters and imposing a 3 degree radial selection from the cluster centre ≈ 18 square degrees. This can be clearly seen in Figure 1. Due to the missing region consisting of mainly the cluster centre, a clear lack of overlap will exist between this and any of the previous bodies of work. As such, this work fails to retrieve many of the previously identified cluster members and so acts to serve as an incremental part of a full cluster survey within the UKIDSS programme.

To retrieve the data from the WSA a similar SQL query to that of Lodieu et al. (2007b) was devised (See Appendix A for the full queries). The query was adapted to cross match with the Sloan Sky Survey through the use of the newly implemented `gcsSourceXDR7PhotoObj` table. The Class parameter in each of the five filter bands was set to only select objects that matched with criteria -2 or -1 in value, i.e. those that had been deemed stellar in nature by the pipeline. While this clearly limits the number of sources by requiring the object to be present in all bands, particularly at the faint end (Lodieu et al. 2007a), it does mean a greater level of reliability for the data that have been selected. Alongside the class selection criteria, the query also placed various quality control mechanisms as defined by the use of the post processing error bits flags on the UKIDSS data and the flags contained within the SDSS subsection².

The SQL query retrieved a total of 79,162 sources from the archive. When asking for the 2MASS and SDSS cross tables, the UKIDSS source identifier was used in order to merge the two separate queries into a master table, with each source containing any data from UKIDSS, 2MASS and/or SDSS. This match was performed using the TOPCAT program in the STARLINK suite of programs. To try and minimise the contamination due to field stars at the outer edges of the survey area where the cluster is more diffuse we employed a radial cut of 3 degrees from the cluster centre. This left 59,779 sources, which we call our GCS dataset.

The objects found by Adams et al. (2002), Chappelle et al. (2005), Hambly et al. (1995b),

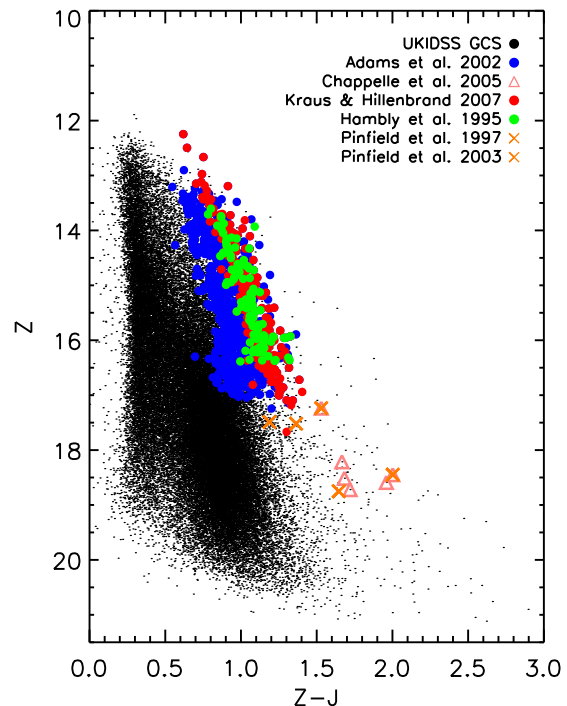


Figure 2. $(Z-J, Z)$ CMD for the ≈ 18 square degrees of the Praesepe cluster selected from the WFCAM Science Archive with a corresponding 2MASS source within the inner 3 degrees of the cluster centre. Matches to this data set from the surveys of Adams et al. (2002), Chappelle et al. (2005), Hambly et al. (1995b), Kraus & Hillenbrand (2007), and Pinfield et al. (1997 and 2003) are also shown. The survey of González-García et al. did overlap with this area however for those sources within the region no matches were found, due possibly to our strict selection criteria on the UKIDSS data.

González-García et al. (2006), Kraus & Hillenbrand (2007), Pinfield et al. (1997) and Pinfield et al. (2003) were then matched to this GCS dataset to select only those whose survey areas overlapped and could be recovered from our data. In total 642 sources were recovered from Adams et al. (who in total report 4,954 objects for their whole survey), 6 from Chappelle et al. (26 in total), 109 from Hambly et al. (515 in total), 0 from González-García et al. (20 in total), 274 from Kraus & Hillenbrand (1,130 in total), and 5 from each of the Pinfield surveys³ these can all be seen in Figure 2.

The first run of the SQL query contained a cross-correlation between the UKIDSS DR6 GCS dataset with its nearest 2MASS counterpart. This cross-correlation allows a determination of proper motion for the matched objects. Typically over a small area the astrometry provided by 2MASS is good to 50 mas (Skrutskie et al. 2006). The CASU pipeline performs its astrometric calibration for the WFCAM data based on point sources within the 2MASS catalogues. Hence, accurate relative proper motions can be derived by simply taking the difference in 2MASS and

² The SDSS flag selections were taken from clean photometry section of the SDSS SQL query sample page <http://cas.sdss.org/dr6/en/help/docs/realquery.asp> Due to the nature of the objects being investigated the constraints were placed only on bands in which the object was likely to be present i.e. The i and z' bands.

³ The objects retrieved from the two Pinfield surveys are the same 5 objects.

WFCAM positions and dividing by the epoch difference (Lodieu et al. 2007b; Jameson et al. 2008). This was automatically done and the results converted into mas yr^{-1} by the SQL query when run through the WSA data centre. The proper motions are described as relative as they exhibit a distinct movement in contrast to the comparably stationary background. The accuracy of the astrometry and the average time baseline of around 5 years provides an error of $\approx 10 \text{ mas yr}^{-1}$. Of the 59,779 sources 34,990 were found to have 2MASS counterparts leaving 24,789 with no 2MASS identifier. Because 2MASS lacks the depth of UKIDSS we only retrieved the brighter of our sample ($K < 16.5$) from this dataset, with the SDSS dataset providing the fainter candidates (The extent of the data set can be seen in Figure 2).

Thanks to the newly implemented `gcSourceXDR7PhotoObj` table linking the WFCAM DR6 and SDSS DR7 data sets at the WSA, a cross-correlation between the UKIDSS data set and that of the SDSS was also available for interrogation. SDSS DR7 reported having surveyed 11,000 square degrees in all of its five filters (*ugriz*) which included the full area of Praesepe (Kraus & Hillenbrand 2007). Upon inspection of the survey dates it became apparent that only a short amount of time had elapsed between the survey of Praesepe by Sloan and that of UKIDSS ($\approx 2 - 2.5$ years on average). The lack of a decent baseline therefore warranted a different approach in order to calculate proper motions and thus cluster membership assignment from that which will be detailed for 2MASS. Again the 59,779 UKIDSS sources were retrieved with 53,562 having an SDSS counterpart and 6,253 being unique to UKIDSS. In total UKIDSS has 2,225 unique sources for which no counterpart has been found in either 2MASS or SDSS (30,998 objects were present in all three surveys).

3 MEMBERS OF PRAESEPE FROM 2MASS

This section will describe the processes undertaken to construct the list of candidate cluster members in Praesepe from the UKIDSS colour magnitude diagrams, and where possible proper motion vector point analysis based from the 2MASS-UKIDSS cross-correlation. The procedure is as follows:

- (i) Select only those sources that have a 2MASS identifier associated with their UKIDSS identifier and are within 3 degrees of the defined cluster centre (34,990 objects).
- (ii) To check the proper motion errors fit the reduced data set (CMD and radius selections imposed) with a two dimensional Gaussian, then use the σ of the Gaussian to act as a proxy for the error.
- (iii) Using the theoretical isochrones, select objects that are no more than 0.3 magnitudes to the left, and all of those on the right in both the (*Z-J,Z*) and (*Y-K,Y*) CMDs.
- (iv) Analyse the resulting Vector Point Diagram (VPD) for this colour selected data set across a range of magnitude bins and inferring from the probability fitting routine a level of cluster membership for each object. Then selecting out a high probability sample (HPM) as those objects with assigned probabilities $p \geq 0.60$.
- (v) Again look at this HPM sample and reject any obvious non-photometric candidates.

3.1 Calculating Proper Motions

The cross-correlation of UKIDSS with 2MASS provided a value for the matched objects proper motion in $\mu_\alpha \cos \delta$ and μ_δ . An estimate of the errors based on the time baseline and specifications of 2MASS is $\approx 10 \text{ mas yr}^{-1}$. To confirm this error estimate, the proper motions for those sources that lay within 3 degrees of the cluster centre (which were spread over a region of proper motion space from -150 to 150 mas yr^{-1}) were divided into bins of 20 mas yr^{-1} and the number in each bin totalled. A two dimensional Gaussian was then fitted enabling, a determination of the cluster spread. Objects that were defined as being outside of the 3σ limit were then removed and the fit reapplied. The σ of the Gaussian then provides an estimate for the error in the proper motions (Jameson et al. 2008) and was found to be of the order of $\approx 12 \text{ mas yr}^{-1}$, instead of our assumed 10 mas yr^{-1} .

3.2 Colour Magnitude Diagrams

In order to select candidates from the CMDs we made use of the BT-NextGen and BT-DUSTY theoretical isochrones which have had the distance modulus of the cluster added to them in order. The models represent different evolutionary paths for describing objects with and without “dusty” atmospheres. Due to the temperatures and masses being explored by this survey the objects involved inhabit both of these regimes and so the two isochrones need to be combined. To create a composite isochrone line, the data points from the BT-NextGen isochrone in the relevant band filter were taken to their minimum temperature $\approx 3000 \text{ K}$. This temperature lies just above where dust grains begin to form in the BD atmosphere and the BT-NextGen models become invalid. We thus combine the BT-DUSTY isochrone models ($T_{\text{eff}} < 3000 \text{ K}$) with the BT-Nextgen models at this point with a simple straight line added in between the resulting break. This composite isochrone was calculated for both the 500 Myr and 1 Gyr evolutionary models due to the uncertainty in the age of Praesepe. It was then employed in both the (*Z-J,Z*) and (*Y-K,Y*) CMDs with sources laying no more than 0.3 magnitudes to the left in the horizontal direction from the line and those to the right being selected and passed to the proper motion fitting routine. See Figure 2 for the VPD and the two CMDs associated with the spatial and colour cut selections. This process selected 7,127 objects out of the possible 34,990. This selection is rather conservative as it aimed to include all the cluster members from the previous surveys, most notably that of Adams et al. (2002) whose objects appear far bluer than those found by both Kraus & Hillenbrand (2007) and by Hambly et al. (1995b).

4 CLUSTER DISTRIBUTIONS AND MEMBERSHIP PROBABILITY

To calculate the membership probabilities for the data sample two distributions were fitted to the cluster. One, a circularly symmetric Gaussian as originally employed by Sanders (1971) and also Francic (1989), and two, an exponential decaying in the direction of the cluster proper motion centre coupled with a perpendicularly oriented Gaussian (Hambly et al. 1995b; Deacon & Hambly 2004). For the

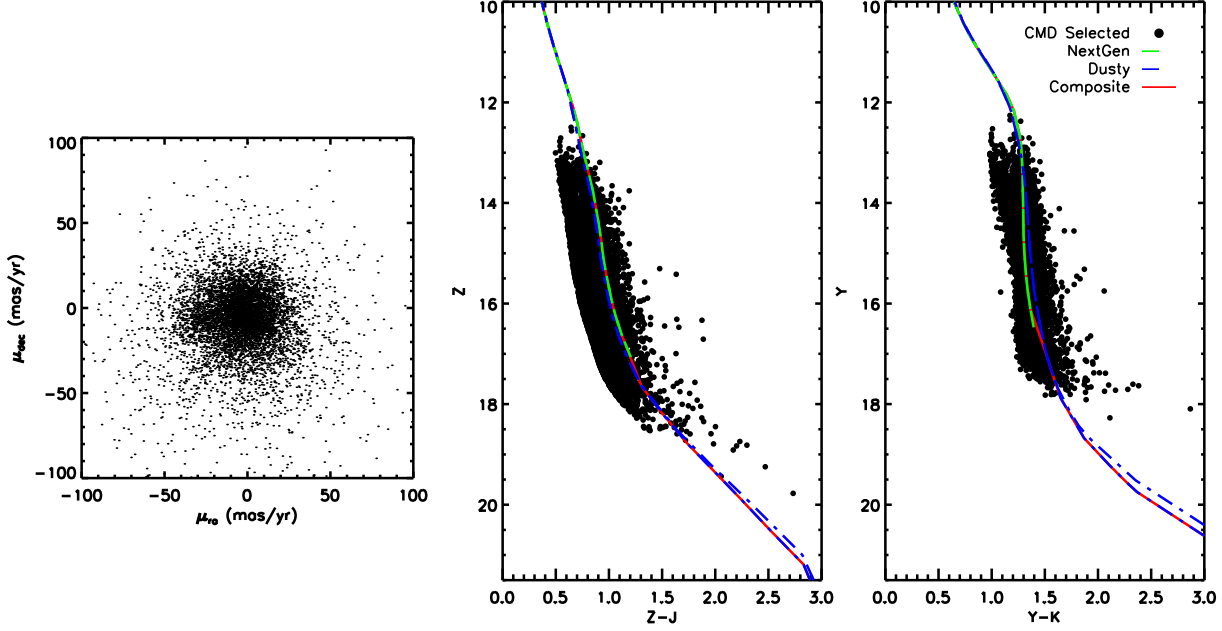


Figure 3. On the left is the VPD for the sources selected from our spatial and colour cuts in the $(Z-J, Z)$ and $(Y-K, Y)$ colour magnitude diagrams as shown in the middle and on the right respectively. The cluster can be seen as the over-density of objects around -30 and -10 mas yr^{-1} in right ascension and declination. The green dashed line is the theoretical isochrone for the BT-NextGen evolutionary model and the blue the BT-DUSTY equivalent. Both the 500 Myr and 1 Gyr flavours have been considered due to the uncertainty in the age of Praesepe.

fitting process to work the cluster proper motion centre $(-35.81, -12.85)$ is rotated from its original position on the Vector Point Diagram to lie on the y-axis. The following set of equations describe the field distribution (Φ_f), cluster distribution (Φ_c) and the normalisation to the exponential (c_o).

$$\Phi_f = \frac{c_o}{\sqrt{2\pi}\Sigma_x} \exp\left(-\frac{(\mu_x - \mu_{xf})^2}{2\Sigma_x^2} - \frac{\mu_y}{\tau}\right). \quad (1)$$

$$\Phi_c = \frac{1}{2\pi\sigma^2} \exp\left(-\frac{(\mu_x - \mu_{xc})^2 + (\mu_y - \mu_{yc})^2}{2\sigma^2}\right). \quad (2)$$

$$c_o = \frac{1}{\tau \left(e^{-\frac{\mu_1}{\tau}} - e^{-\frac{\mu_2}{\tau}} \right)}. \quad (3)$$

Where,

$$c_o \int_{\mu_1}^{\mu_2} e^{-\frac{\mu_y}{\tau}} d\mu_y = 1. \quad (4)$$

The values of μ_x and μ_y refer to the proper motion attributed to each individual object. The quantity σ is the Gaussian width, whilst μ_{xc} and μ_{yc} are the cluster's mean proper motion. Σ_x is the proper motion dispersion value in x and τ the exponential scale length for the field proper motion distribution in y . μ_{xf} is the field mean proper motion in x and finally μ_1 and μ_2 are the limits for the normalisation to the exponential c_o . For the rotated VPD these were set at 20 and 70 mas yr^{-1} to avoid the mass of stars centred around (0,0).

Combining the field star distribution and the cluster distribution with information about the fraction of stars

which are field stars (f) the resulting expression for the total distribution (Φ) is

$$\Phi = f\Phi_f + (1 - f)\Phi_c. \quad (5)$$

After employing the method of maximum likelihood with Θ representing one of the free parameters,

$$\sum_i \frac{\delta \ln \Phi_i}{\delta \Theta} = 0, \quad (6)$$

a set of nonlinear equations can be defined as the following.

$$f : \sum_i \frac{\Phi_f - \Phi_c}{\Phi} = 0, \quad (7)$$

$$\sigma : \sum_i \frac{\Phi_c}{\Phi} \left(\frac{(\mu_x - \mu_{xc})^2 + (\mu_y - \mu_{yc})^2}{\sigma^2} - 2 \right) = 0, \quad (8)$$

$$\Sigma_x : \sum_i \frac{\Phi_f}{\Phi} \left(\frac{(\mu_x - \mu_{xf})^2}{\Sigma_x^2} - 1 \right) = 0, \quad (9)$$

$$\mu_{xf} : \sum_i \frac{\Phi_f}{\Phi} (\mu_x - \mu_{xf}) = 0, \quad (10)$$

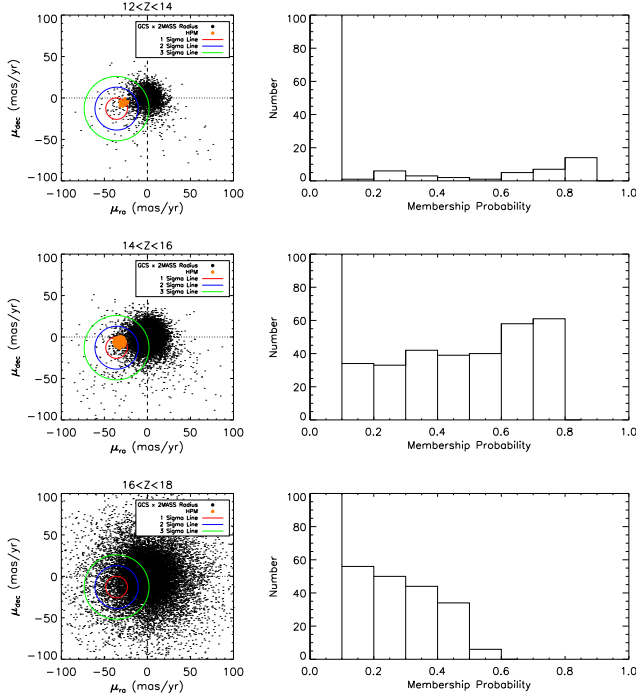
$$\mu_{xc} : \sum_i \frac{\Phi_c}{\Phi} (\mu_x - \mu_{xc}) = 0, \quad (11)$$

$$\mu_{yc} : \sum_i \frac{\Phi_c}{\Phi} (\mu_y - \mu_{yc}) = 0, \quad (12)$$

$$\tau : \sum_i \frac{\Phi_f}{\Phi} \left(\frac{\mu_y}{\tau} - 1 - c_o(\mu_1 e^{-\frac{\mu_1}{\tau}} - \mu_2 e^{-\frac{\mu_2}{\tau}}) \right) = 0. \quad (13)$$

Table 1. Fitted parameter values for the set of magnitude bins analysed by the VPD-Probability Fitting Routine.

Interval	f	σ	μ_{xc}	μ_{yc}	τ	Σ_x	μ_{xf}
12.00 < Z < 14.00	0.75	3.28	3.53	27.73	21.46	18.94	-5.43
14.00 < Z < 16.00	0.71	5.45	4.43	30.65	14.26	18.89	-4.00
16.00 < Z < 18.00	0.89	5.43	-0.27	31.87	14.91	19.54	-1.95

**Figure 4.** Proper Motion vector point diagrams and the resulting probability histograms for each magnitude interval in the probability fitting of the Praesepe data. In each plot the three coloured lines represent the 1σ , 2σ and 3σ errors obtained from our estimate of proper motion errors by way of the 2D Gaussian fit, they have been shifted to be located over the clusters proper motion centre. The points in orange show our high probability sample.

To each of these equations a bi-section algorithm was devised that checks for root bracketing and then proceeds to find the root to the desired level of accuracy. Once one parameter has been fitted, the next parameter is subject to the same process. Finally once τ has been found the process reverts back to its starting point and runs again until all the free parameters have been fixed (showing no further sign of deviation). To start the process a set of initial values is required for the free parameters, these are as in Deacon & Hambly (2004). Once the values are fixed the membership probabilities for the i^{th} object can be calculated thus;

$$p_i = \frac{(1-f)\Phi_{ci}}{\Phi_i}. \quad (14)$$

The fitted values for each magnitude interval are shown in Table 1 and vector point diagrams and probability histograms in Figure 4. Taking the sigma value of the Gaussian from section 3.1 and placing it over the cluster's centre of proper motion we find 380 objects with a probability as-

signment. Of these, 121 have probabilities that place them in the High Membership bracket ($p > 0.60$). In total 145 sources are found to have a $p \geq 0.60$. The 24 laying outside the sigma selection are still very much consistent with the cluster as can be seen by small spread of objects proper motion space in Figure 4.

5 MEMBERS OF PRAESEPE FROM SDSS

In this section the process for locating any possible candidates/members of the Praesepe cluster from available data within the cross link between UKIDSS and SDSS will be described.

- (i) Select those objects that are again within the 3 degree radial cut from the cluster centre. These objects are only present in UKIDSS-SDSS data set Any corresponding SDSS-2MASS source would have been treated within the previous section.
- (ii) Select the list of candidate objects from 6 CMDs.
- (iii) Extract the FITS files for these objects from the WSA and SDSS Data Access Server.
- (iv) Calculate a pixel to pixel transformation between the two images and using the epoch difference calculate a proper motion.
- (v) Perform a basic probability analysis on the resulting data.

5.1 Extracting the Candidates

Performing the same radial cut with objects only present in the UKIDSS-SDSS match (no 2MASS counterpart) led to a selection of 22,564 objects. To extract the candidates from this list, a series of photometric cuts were applied in a range of different CMDs. These can be seen in Figure 5. These CMDs made use of a range of different filters and known locations of LMS/VLMS and BDs as detailed by Hawley et al. (2002). Objects within these predefined regions were selected for further analysis.

5.2 Refinement of Proper Motions

The primary problem with the SDSS dataset is the small epoch difference between the two surveys which subsequently results in large errors on the proper motion. This, coupled with a small number of objects (< 100) means that the analysis as performed for the 2MASS data is not applicable. An alternate approach has therefore been taken in order to assign membership probabilities to these candidates. To begin with, suitable queries were developed to allow the acquisition of the catalogue and fits flat files from each survey's

Table 2. Probability of membership, magnitude range for our methods of calculating probabilities of membership using the annulus as well as the two control areas.

Magnitude Range	Probability Annulus	Probability	
		$\mu_\alpha=0 \text{ mas yr}^{-1}$ $\mu_\delta=+37.85 \text{ mas yr}^{-1}$	$\mu_\alpha=+35.66 \text{ mas yr}^{-1}$ $\mu_\delta=-12.70 \text{ mas yr}^{-1}$
15 < Z < 16	0.000	0.000	0.000
16 < Z < 17	0.000	0.000	0.000
17 < Z < 18	0.000	0.000	0.000
18 < Z < 19	0.000	1.000	0.000
19 < Z < 20	0.581	0.500	1.000
20 < Z < 21	0.000	0.000	0.000

data centre⁴. The candidate object were then located and a set of reference objects selected. These reference objects had to be common to both chips (appearing in each epoch), be in the magnitude range $12.0 < Z < 18.0$, have ellipticities less than 0.2 (from UKIDSS catalogue data) and not sit within 5% of the chip border (in pixels) in order to help minimise any radial distortion effects.

The list of reference objects are used to create a 12 parameter transformation (where too few reference objects were present for the quadratic fit a linear 6 parameter fit was tried instead) that allows the motion of the candidate object between the two epochs to be calculated. Reference objects that are shown to be moving at a rate greater than 3 times the rms value of the fit are discarded. The revised reference list is again passed to the fitting routines in order to calculate the correct coefficients that describe the motion between the two epochs. This motion is then converted into mas yr^{-1} through the use of the following equations;

$$\mu_\alpha = \frac{((CD1.1 \times \Delta x + \Delta y \times CD1.2) \times 3600 \times 1000)}{\text{epoch_difference}}, \quad (15)$$

$$\mu_\delta = \frac{((CD2.1 \times \Delta x + \Delta y \times CD2.2) \times 3600 \times 1000)}{\text{epoch_difference}}. \quad (16)$$

The quantities $CD1.1$, $CD1.2$, $CD2.1$ and $CD2.2$ are the world co-ordinate transformation matrix elements contained within the FITS header (Greisen & Calabretta 2002), whilst Δx and Δy simply refer to the change in pixel elements. The direction in μ_α is finally further corrected by multiplying by the appropriate $\cos\delta$ value.

In order to calculate errors, the magnitudes of all possible objects were calculated on the reference image frames using the relevant calculations listed on the SDSS⁵ and WSA⁶ pages. The x and y pixel centroiding errors reported for each object in the catalogue files were then totalled for each bin of width two magnitudes and divided by the number in that magnitude bin to give an average centroiding uncertainty value. These values were then added in quadrature with the

rms in that particular direction as found by the 12 parameter quadratic fit.

$$\text{error_pm} = \sqrt{\text{rms}^2 + \text{err}_{\text{epoch1}}^2 + \text{err}_{\text{epoch2}}^2} \quad (17)$$

The values representing the error found in the x or y direction for both epoch 1 and epoch 2 measurements are in turn calculated from the following;

$$\mu_{\alpha\text{-err}} = \frac{((CD1.1 \times \text{xerr} + \text{yerr} \times CD1.2) \times 3600 \times 1000)}{\text{epoch_difference}} \quad (18)$$

$$\mu_{\delta\text{-err}} = \frac{((CD2.1 \times \text{xerr} + \text{yerr} \times CD2.2) \times 3600 \times 1000)}{\text{epoch_difference}} \quad (19)$$

where xerr and yerr represent the centroiding errors in the x and y directions as described in the previous paragraph. The errors on the proper motion are likely an over-estimation of the astrometric errors as they are based on the rms from the fitting process rather than an error in the transformed coordinate.

To try and calculate membership probabilities for these objects, an attempt at using control data to determine levels of contamination was undertaken. The cluster circle and two control circles of radius 26" were used. The radius value is the average value taken from the 12 parameter fit information, ignoring any obvious discrepancies (as objects become fainter the centroiding errors become larger). Those that were in the faintest magnitude bin had centroiding errors a factor ten larger than for the other candidates and so were discounted from the average). The circles were located at the same distance from (0,0) in proper motion space and as is usual, the data were split into magnitude bins with the probability being calculated using equation 20.

$$P_{\text{membership}} = \frac{N_{\text{cluster}} - N_{\text{control}}}{N_{\text{cluster}}}. \quad (20)$$

$P_{\text{membership}}$ is the probability assigned for a particular magnitude bin, N_{cluster} the number of field and cluster stars within the cluster circle and N_{control} the number of field stars. Thus $N_{\text{cluster}} - N_{\text{control}}$ should give the number of Praesepe members. One flaw to this method as reported by Casewell et al. (2007) is that this method is dependent on the chosen location of the control circle. A solution to correct this is to use the field star count within the annulus of Figure 6 and scale this to the area of the cluster circle to estimate levels of contamination. The resulting probabilities for the control circles and annulus are reported in Table 2. Any negative probabilities have been altered to 0.00. The only magnitude bin to contain a positive probability is

⁴ For the SDSS data this involved creating a few specific requests as the catalogue data is split amongst a wide range of files. The SDSS DAS has also recently been updated to SDSS DAS Version 2 for use with DR7, users are instructed to read the DR7 release website for more information.

⁵ SDSS Magnitude Algorithm calculations:
<http://www.sdss.org/dr6/algorithms/fluxcal.html#counts2mag>

⁶ WFCAM Magnitude Algorithm calculations:
<http://surveys.roe.ac.uk/wsa/flatFiles.html#catmags>

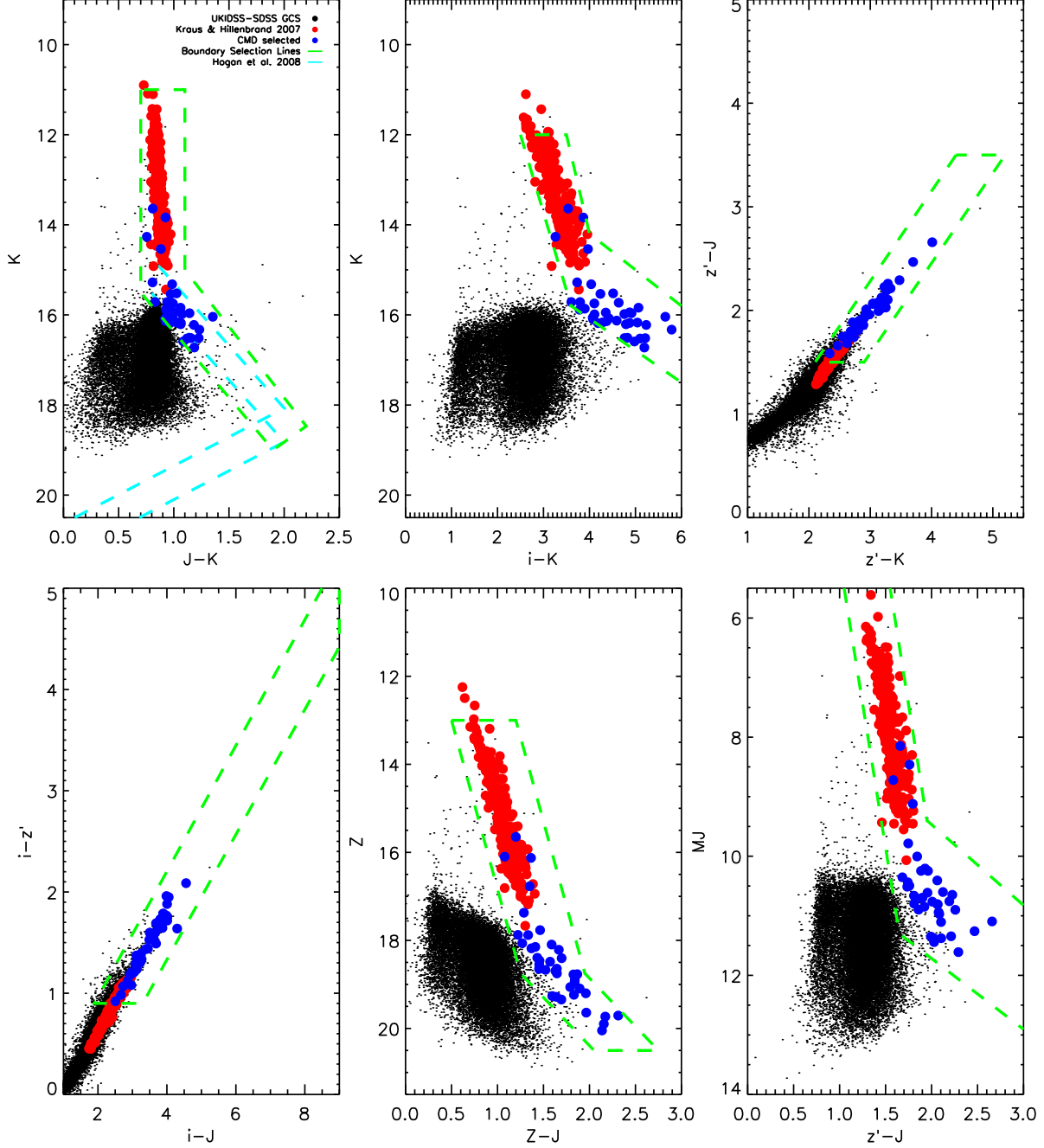


Figure 5. CMDs for SDSS and UKIDSS photometric bands showing the selection regions (as denoted by the green dashed lines) used to extract the set of 39 candidate objects as shown by the blue circles. The objects of Kraus & Hillenbrand (2007) shown in red have been used alongside information from plots in figure 9 of Hawley et al. (2002) to denote the appropriate regions for the cluster sequence. Additionally the cluster sequence for the Hyades (a cluster of similar age to Praesepe) as found by Hogan et al. (2008) has been corrected for the distance of Praesepe and over plotted in the $J-K$, K plot (blue dashed line) to help trace any possible cluster sequence. The black dots are the UKIDSS-SDSS sources that are not present in the UKIDSS-2MASS population.

the bin $19 < Z \leq 20$, for which the control data revealed a probability of 0.5 and 1.0. The annulus method for the same magnitude bin put the probability at 0.58. These membership probabilities should be viewed with caution as the low numbers (i.e. few objects) make the probabilities difficult to fully substantiate. As such, objects in these fainter magnitude bins have not been taken into consideration when

constructing the luminosity and mass functions reported in section 6. When the survey of the cluster centre is complete it is hoped that not only will more LMS/BD candidates be found but that the increase in numbers will also allow for a more robust membership probability to be assigned.

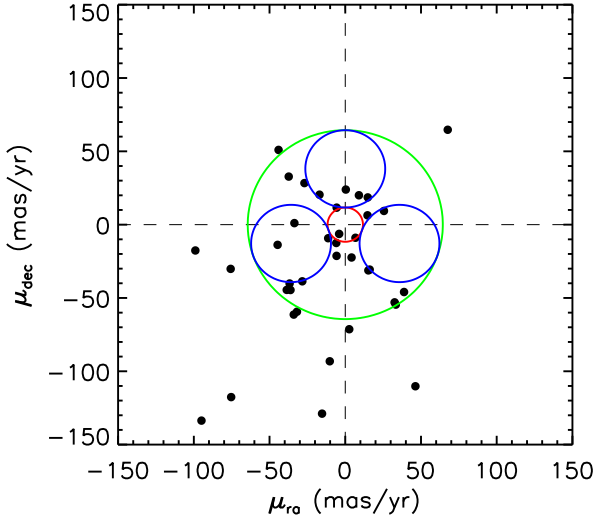


Figure 6. Proper motion vector diagram for the 39 UKIDSS-SDSS candidate objects selected from the photometric cuts. The cluster location is at $\mu_\alpha = -35.81 \text{ mas yr}^{-1}$ & $\mu_\delta = -12.85 \text{ mas yr}^{-1}$ with the two control circles and the annulus used for the second measure of probability also plotted. None of these objects are included in the luminosity and mass function analysis.

6 CLUSTER MASS AND LUMINOSITY FUNCTIONS

In order to produce the luminosity function of the cluster the effects of incompleteness on the data must be taken into account. As magnitude increases, the number of objects in a specified magnitude bin of uniform distribution will also increase. Counting the number of stars present and comparing it to this predicted rate of growth will show up any signs of incompleteness. This is done by taking the logarithm of the number of stars in the magnitude bin and fitting a best fit line to the data up until this “drop off” point. An estimate for the level of incompleteness is calculated from the deficit. For the purposes of this study the best fit line was fitted between the black points in Figure 7 for the UKIDSS-2MASS data set in the Z , J and K filters. The drop off can be clearly seen at the fainter magnitudes with the brighter magnitude drop off likely caused by bright cut off limit of the surveys.

The cluster luminosity function (Figure 8) was calculated by summing the assigned membership probabilities of each object in bins of width one magnitude. Each interval was then multiplied by the incompleteness factor, producing the correction from the dashed blue to solid black lines. In order to avoid distorting the luminosity function we applied this process to the UKIDSS-2MASS population only. The fainter magnitudes and tentative membership probabilities of the UKIDSS-SDSS candidates excluded them, as inappropriately large correction factors would have to be applied. The luminosity function can be seen to have a clear and well defined peak in each of the filters followed by a decrease due to a change in slope of the mass-luminosity relationship. The first point in the J -band luminosity function has been artificially raised due to an large incompleteness factor being

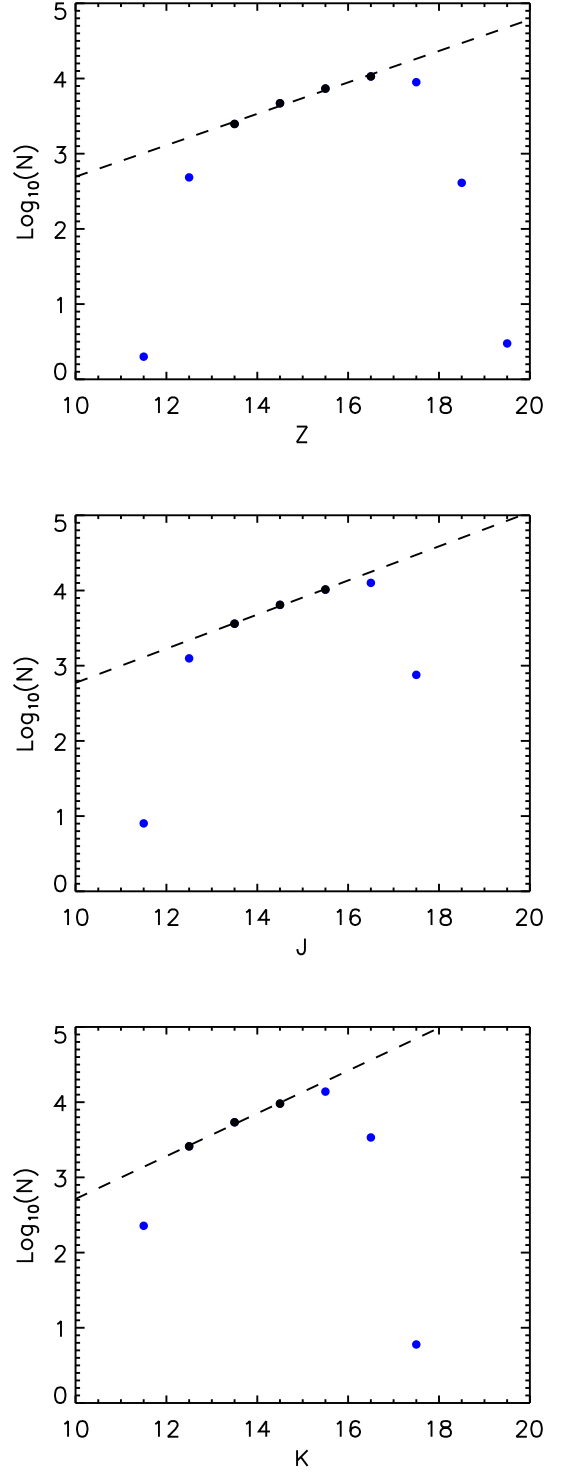


Figure 7. An estimate of the incompleteness in the 2MASS selected Praesepe data set for the UKIDSS Z , J and K bands respectively. The black dotted line is a least squares fit to the associated black points in figure. There is clearly a drop off at the end of the functions whilst the deficit for the brightest magnitude bins is caused by saturation effects.

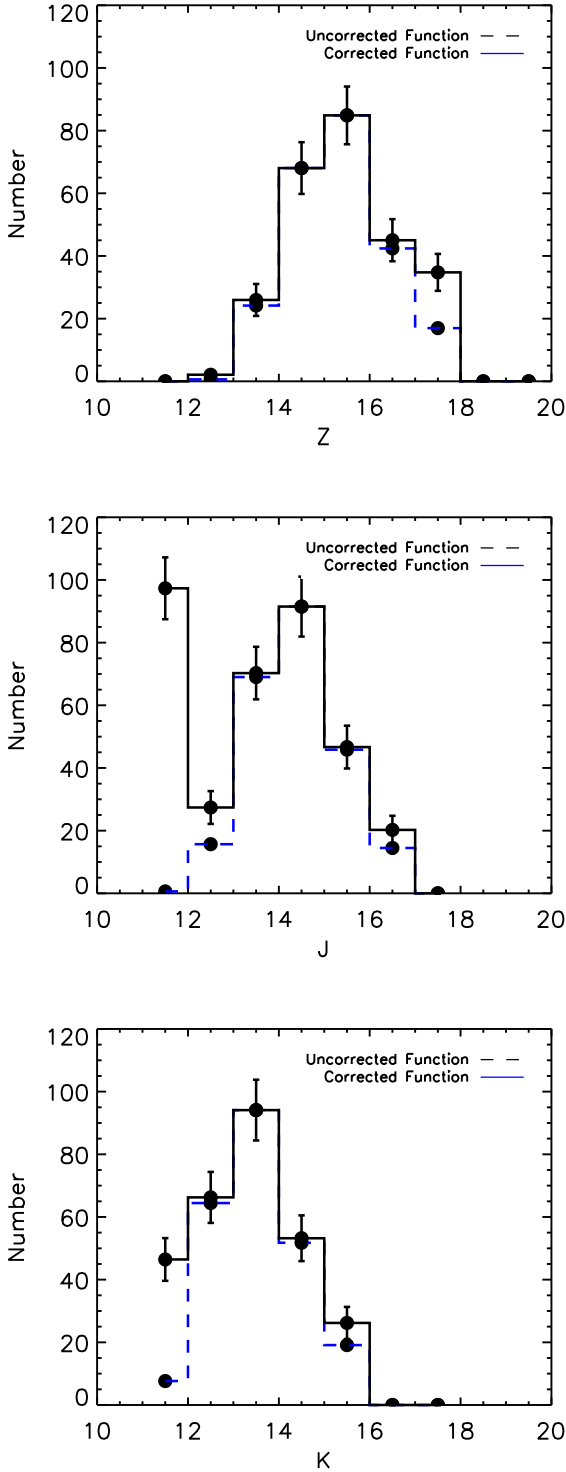


Figure 8. The Luminosity Functions derived for the Praesepe star cluster in the Z , J and K bands. The distribution rises to a peak before starting to decay due to the change in the slope of the mass-luminosity relationship. The error bars are Poisson errors.

applied. This point is thus not treated when fitting the mass function. The errors shown are simply Poisson errors.

To convert the cluster luminosity function into a mass function a mass-luminosity relationship is required (see Figure 9). Again a combined relationship formed from the BT-NextGen and BT-DUSTY models was constructed. Cubic spline interpolation was used to interpolate between the points. As the age of the Praesepe cluster is not well confined this mass-luminosity relationship has again been constructed based of both the 500 Myr and 1 Gyr model data.

If one considers a magnitude interval of width dM the total number of stars (dN) will be given by

$$dN = \Phi(M)dM \quad (21)$$

where $\Phi(M)$ is the luminosity function. In the corresponding mass interval the same dN is now given by $\xi(m)dm$, where dm is the interval in the mass range and $\xi(m)$ is the mass function.

Hence to calculate the mass function the previous equations can be easily rearranged to the form of

$$\xi(m) = \frac{\Phi(M)dM}{dm} \quad (22)$$

In Figure 10, Praesepe's cluster mass function is plotted with a single power law fit for the points between 0.6 and 0.125 M_{\odot} for the Z photometric band. The J and K bands have been treated similarly but due to the corrections applied for the incompleteness affecting a wider range of magnitudes a narrower mass range was considered. The form of the power law is shown below.

$$\xi(m) \propto m^{-\alpha} \quad (23)$$

The results of this fitting are that $\alpha_{500Myr}=1.11 \pm 0.37$ and $\alpha_{1Gyr}=1.10 \pm 0.37$. For the J and K bands the results were $\alpha_{500Myr}=1.07$, $\alpha_{1Gyr}=1.07$ and $\alpha_{500Myr}=1.09$, $\alpha_{1Gyr}=1.09$ respectively. These values are much lower than the Salpeter IMF (2.35) but the upper limits agree roughly with the values calculated and cited by Kraus & Hillenbrand (2007) of $\alpha=1.4 \pm 0.2$. The Kraus & Hillenbrand result was derived using a mass-spectral type relationship, however after retrieving 2MASS J band photometry for their objects and constructing the J band luminosity function as we have done for our UKIDSS-2MASS sample we find α to differ by only 0.1.

A more recent survey of the cluster centre has also just been carried out by Boudreault et al. (2009). The authors identify some 150 candidate members with 6 expected to be BDs. Of these 6 only 3 are currently within our survey region, objects 55, 909 and 910. Objects 55 and 909 are precluded from our search due to their morphological classification in the UKIDSS data. Object 910 is present and photometrically appears to agree with Boudreault et al. ($J = 17.66$, $K = 16.8$). The presence of other photometric bands has however shown this object to be far too blue in the Z - J , J diagram ($Z = 18.33$) for it to be considered as a cluster member by our current analysis. The value presented by Boudreault et al. of $\alpha = 1.8 \pm 0.1$ for $\xi(m)$ (the mass function) appears to be much greater than our calculated value and more in line with the upper value presented by Kraus & Hillenbrand. The survey however does not use proper motion information and restricts its objects to candidates with uniform probability of membership ($p=1.0$). Ob-

Table 3. Mass function results from previous surveys

Survey	Passband	Mass range	Slope
Baker et al.	<i>Z</i>	0.125 - 0.6 M_{\odot}	1.10 ± 0.37
Baker et al.	<i>J</i>	0.20 - 0.5 M_{\odot}	1.07
Baker et al.	<i>K</i>	0.20 - 0.5 M_{\odot}	1.09
Kraus and Hillenbrand	SED ^a	0.17 - 1 M_{\odot}	1.4 ± 0.2
Boudreault et al.	<i>J</i>	0.10 - 0.7 M_{\odot}	2.3 ± 0.2
Boudreault et al.	<i>J</i>	0.18 - 0.45 M_{\odot}	1.8 ± 0.1

^a See the appendix of for a discussion on how the multiple photometric bands coupled with theoretical models were used to derive masses for each spectral type.

taining the *J* band photometry of the 150 Boudreault et al. objects and treating them in the same manner again with our luminosity-mass relationship confirms their result as we find $\alpha = 1.85 \pm 0.15$. See Table 3 for a summary of the results. It is important then that a full survey including the more densely populated centre takes place as this would likely increase the number of members found (particularly at the lower mass end) thus altering the IMF that would be observed. The full extent of this change is of course unknown. It is clear however that even with a more complete data set there are likely to be few BDs within the Praesepe cluster. This is consistent with a cluster of such age having undergone many cycles of equipartition of energy, so ejecting low mass objects from the cluster. The true record breakers in the low mass stakes will therefore be found as companions to other objects as the combined system mass would restrict the amount ejected through dynamical events

7 SUMMARY

A study of available UKIDSS data on the Praesepe star cluster combined with archive data from the 2MASS and SDSS surveys for the range of $12 \leq Z < 21$ has found, through a combination of proper motion and colour magnitude diagram selections 145 HPM (see Figure 11 and Appendix B), of which, 14 appear to be new members, Appendix C. The majority of the detected HPM objects have also been found in more than one previous body of work, almost certainly confirming their status as cluster members. These objects all inhabit a fairly bright magnitude region on the cluster sequence as they have been derived from investigation the brighter UKIDSS-2MASS data set. The UKIDSS-SDSS data set, whilst allowing fainter objects to be examined, suffers from a short time base between observations and small number statistics making membership assignments difficult to quantify (see Appendix D for a list of the candidate objects). An investigation into the cluster luminosity and hence mass function was also carried out. The upper limits of the later agree with a previous result given by Kraus & Hillenbrand (2007), confirming that although a low mass population of objects may have existed the dynamical evolution of the cluster over its lifetime has led to a significant population depletion. Only when a full survey of the cluster with UKIDSS is complete and second epoch *K* data available can one hope to truly evaluate this cluster.

8 ACKNOWLEDGEMENTS

DEAB acknowledges the support of an STFC Postgraduate studentship. NL was supported by the Ramón y Cajal fellowship number 08-303-01-02. This publication makes use of data products from the United Kingdom Infrared Deep Sky Survey, the Sloan Digital Sky Survey, the Two Micron All Sky Survey, the SIMBAD database, operated at CDS, Strasbourg, France and NASA's Astrophysics Data System Bibliographic Services. The SDSS is managed by the Astrophysical Research Consortium (ARC) for the Participating Institutions. The Participating Institutions are The University of Chicago, Fermilab, the Institute for Advanced Study, the Japan Participation Group, The Johns Hopkins University, Los Alamos National Laboratory, the Max-Planck-Institute for Astronomy (MPIA), the Max-Planck-Institute for Astrophysics (MPA), New Mexico State University, University of Pittsburgh, Princeton University, the United States Naval Observatory, and the University of Washington. Funding for the Sloan Digital Sky Survey (SDSS) has been provided by the Alfred P. Sloan Foundation, the Participating Institutions, the National Aeronautics and Space Administration, the National Science Foundation, the U.S. Department of Energy, the Japanese Monbukagakusho, and the Max Planck Society. The SDSS Web site is <http://www.sdss.org/>. The Two Micron All Sky Survey, is a joint project of the University of Massachusetts and the Infrared Processing and Analysis Center/California Institute of Technology, funded by the National Aeronautics and Space Administration and the National Science Foundation. The authors would like to thank France Allard for the use of the Phoenix web simulator at <http://phoenix.ens-lyon.fr/simulator/index.faces> which has been used in this research.

REFERENCES

- Adams J. D., Stauffer J. R., Skrutskie M. F., Monet D. G., Portegies Zwart S. F., Janes K. A., Beichman C. A., 2002, *AJ*, 124, 1570
- Allen C. W., 1973, *Astrophysical quantities*, Allen C. W., ed.
- Baraffe I., Chabrier G., Allard F., Hauschildt P. H., 1998, *A&A*, 337, 403
- Boudreault S., Bailer-Jones C. A. L., Goldman B., Henning T., Caballero J. A., 2009, *ArXiv e-prints*
- Burrows A., Hubbard W. B., Lunine J. I., Liebert J., 2001, *Reviews of Modern Physics*, 73, 719
- Casali M., et al., 2007, *A&A*, 467, 777

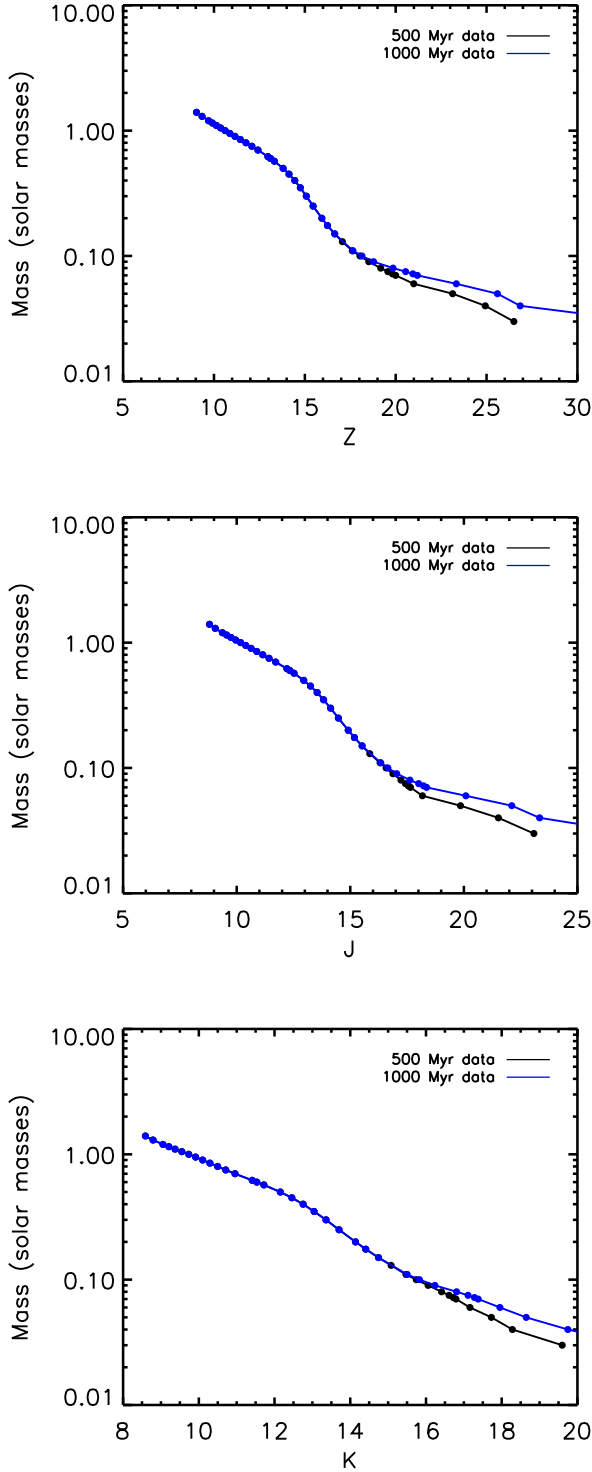


Figure 9. The mass-luminosity relationship used in this study is based off a composite BT-NextGen and BT-DUSTY line with a cubic spline interpolation. The black points represent the 500 Myr data whilst the blue the 1 Gyr data. The lines only start to deviate appreciably at faint magnitudes, which we do not investigate. Shown here is the mass-luminosity relationship for the Z , J and K bands respectively.

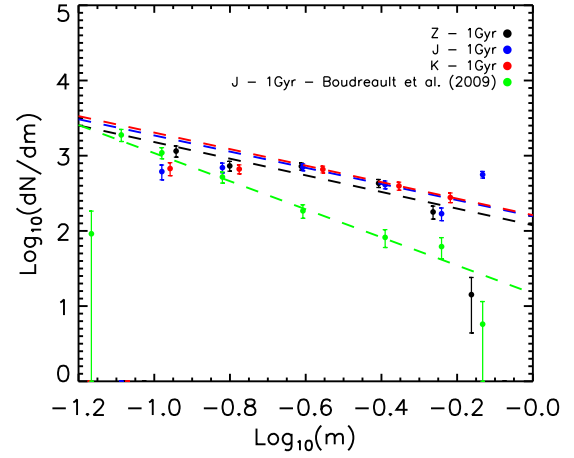


Figure 10. The derived cluster mass function with the power law fit for the Z photometric band shown in dashed black. The fits for the J and K bands are also shown in blue and red respectively. The green points are taken from Boudreault et al. (2009). The error bars are Poisson errors. For clarity only the 1 Gyr data and fit has been plotted as there is little deviation between that and the 500 Myr fit.

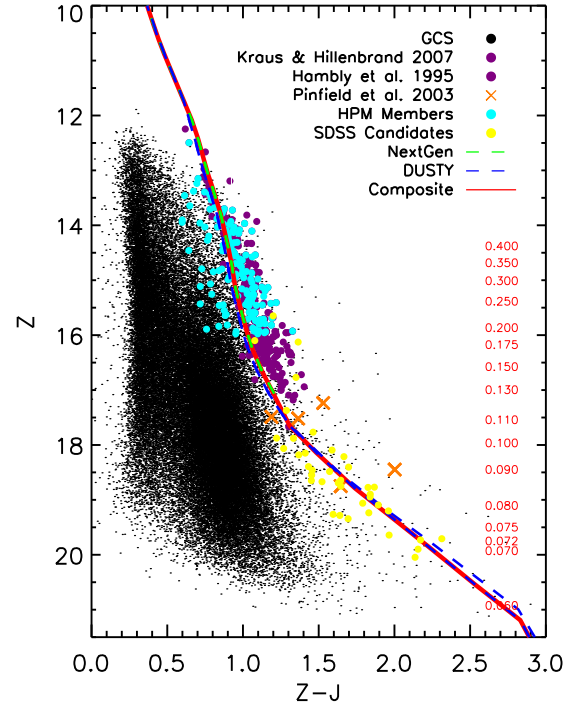


Figure 11. A Z - J , Z CMD showing the cluster members given by Hambly et al. and Kraus & Hillenbrand alongside the 145 HPM derived from this work. The BT-NextGen, BT-DUSTY and composite selection lines are also shown as are the masses (in units of solar mass) given by those models for the 500 Myr case. The candidate UKIDSS-SDSS members are also shown to show the limits of the survey. Most of the UKIDSS-SDSS objects were found in this analysis to be non-members.

- Casewell S. L., Dobbie P. D., Hodgkin S. T., Moraux E., Jameson R. F., Hambly N. C., Irwin J., Lodieu N., 2007, *MNRAS*, 378, 1131
- Chabrier G., Baraffe I., Allard F., Hauschildt P., 2000, *ApJ*, 542, 464
- Chappelle R. J., Pinfield D. J., Steele I. A., Dobbie P. D., Magazzù A., 2005, *MNRAS*, 361, 1323
- de La Fuente Marcos R., de La Fuente Marcos C., 2000, *Ap&SS*, 271, 127
- Deacon N. R., Hambly N. C., 2004, *A&A*, 416, 125
- Eggen O. J., 1960, *MNRAS*, 120, 540
- Francis S. P., 1989, *AJ*, 98, 888
- Girardi L., Bertelli G., Bressan A., Chiosi C., Groenewegen M. A. T., Marigo P., Salasnich B., Weiss A., 2002, *A&A*, 391, 195
- González-García B. M., Zapatero Osorio M. R., Béjar V. J. S., Bihain G., Barrado Y Navascués D., Caballero J. A., Morales-Calderón M., 2006, *A&A*, 460, 799
- Greisen E. W., Calabretta M. R., 2002, *A&A*, 395, 1061
- Hambly N. C., Steele I. A., Hawkins M. R. S., Jameson R. F., 1995a, *MNRAS*, 273, 505
- , 1995b, *A&AS*, 109, 29
- Hambly N. C., et al., 2008, *MNRAS*, 384, 637
- Hawley S. L., et al., 2002, *AJ*, 123, 3409
- Henry R. C., Anderson R., Hesser J. E., 1977, *ApJ*, 214, 742
- Hewett P. C., Warren S. J., Leggett S. K., Hodgkin S. T., 2006, *MNRAS*, 367, 454
- Hodgkin S. T., Irwin M. J., Hewett P. C., Warren S. J., 2009, *MNRAS*, 394, 675
- Hogan E., Jameson R. F., Casewell S. L., Osbourne S. L., Hambly N. C., 2008, *MNRAS*, 728
- Irwin M. J., et al., in preparation
- Jameson R. F., Casewell S. L., Bannister N. P., Lodieu N., Keresztes K., Dobbie P. D., Hodgkin S. T., 2008, *MNRAS*, 384, 1399
- Jones B. F., Cudworth K., 1983, *AJ*, 88, 215
- Kharchenko N. V., Piskunov A. E., Röser S., Schilbach E., Scholz R., 2005, *A&A*, 438, 1163
- Klein-Wassink W. J., 1927, *Groningen Publ. No. 41 (KW)*, 41
- Kraus A. L., Hillenbrand L. A., 2007, *AJ*, 134, 2340
- Lawrence A., et al., 2007, *MNRAS*, 379, 1599
- Lodieu N., Dobbie P. D., Deacon N. R., Hodgkin S. T., Hambly N. C., Jameson R. F., 2007a, *MNRAS*, 380, 712
- Lodieu N., Hambly N. C., Jameson R. F., Hodgkin S. T., Carraro G., Kendall T. R., 2007b, *MNRAS*, 374, 372
- Monet D. G., et al., 2003, *AJ*, 125, 984
- Pinfield D. J., Dobbie P. D., Jameson R. F., Steele I. A., Jones H. R. A., Katsiyannis A. C., 2003, *MNRAS*, 342, 1241
- Pinfield D. J., Hodgkin S. T., Jameson R. F., Cossburn M. R., von Hippel T., 1997, *MNRAS*, 287, 180
- Sanders W. L., 1971, *A&A*, 14, 226
- Skrutskie M. F., et al., 2006, *AJ*, 131, 1163
- Tsvetkov T. G., 1993, *Ap&SS*, 203, 247
- van Leeuwen F., 2009, *A&A*, 497, 209
- Vandenberg D. A., Bridges T. J., 1984, *ApJ*, 278, 679
- York D. G., et al., 2000, *AJ*, 120, 1579
- Zacharias N., Urban S. E., Zacharias M. I., Wycoff G. L., Hall D. M., Monet D. G., Rafferty T. J., 2004, *AJ*, 127, 3043

APPENDIX A: SQL QUERIES**A1 UKIDSS-SDSS**

```

SELECT
g.sourceID as u_id,
T2.slaveObjID as s_id,
g.ra as u_ra,
g.dec as u_dec,
T2.ra as s_ra,
T2.dec as s_dec,
m.mjdObs as u_mjd,
T2.mjd_z as s_mjd,
g.mergedClass as u_class,
g.zaperMag3 as u_z,
g.zaperMag3Err as u_zerr,
g.yaperMag3 as u_y,
g.yaperMag3Err as u_yerr,
g.japerMag3 as u_j,
g.japerMag3Err as u_jerr,
g.haperMag3 as u_h,
g.haperMag3Err as u_herr,
g.k_laperMag3 as u_k,
g.k_laperMag3Err as u_kerr,
T2.psfMag_u as s_u,
T2.psfMagErr_u as s_uerr,
T2.psfMag_g as s_g,
T2.psfMagErr_g as s_gerr,
T2.psfMag_r as s_r,
T2.psfMagErr_r as s_rerr,
T2.psfMag_i as s_i,
T2.psfMagErr_i as s_ierr,
T2.psfMag_z as s_z,
T2.psfMagErr_z as s_zerr,

(T2.distanceMins * 60) as us_separation,

3.6e6*COS(RADIANS(g.dec))*(g.ra-T2.ra)/((m.mjdObs-T2.mjd_z)/365.25) AS us_pmra,
3.6e6*(g.dec-T2.dec)/((m.mjdObs-T2.mjd_z)/365.25) AS us_pmdec,

g.framesetid as framesetid,
f.multiframeid as multiframeid,
m.filename as filename,
m.catname as catname,
f.extNum as extnum,
T2.run as run,
T2.rerun as rerun,
T2.camcol as camcol,
T2.field as field,
T2.rowc_z as xpix,
T2.colc_z as ypix,
T2.segmentID as segmentID,
T2.stripe as stripe,
T2.chunkID as chunkID,
T2.startmu as startmu

FROM
gcsMergeLog as ml,
Multiframe as m,
gcsFrameSets as f,
(
SELECT sdss.ra, sdss.dec, x.slaveObjID, x.masterObjID, x.distanceMins,
sdss.psfMag_u, sdss.psfMagErr_u, sdss.psfMag_g, sdss.psfMagErr_g, sdss.psfMag_r, sdss.psfMagErr_r,

```

```
sdss.psfMag_i, sdss.psfMagErr_i, sdss.psfMag_z, sdss.psfMagErr_z, f.mjd_z, sdss.run, sdss.rerun,
sdss.camcol, sdss.field, sdss.rowc, sdss.colc, sg.segmentID, sg.stripe, c.chunkID, c.startmu
```

```
FROM gcsSourceXDR7PhotoObj as x, BestDR7..PhotoObj as sdss,
BestDR7..Field as f, BestDR7..Segment as sg, BestDR7..Chunk as c
```

```
WHERE sdss.type = 6 AND x.slaveObjID = sdss.objID AND f.fieldID = sdss.fieldID
AND f.segmentID = sg.segmentID AND sg.chunkID = c.chunkID
```

```
/* Detected in BINNED 1 */
AND ((flags_i & 0x10000000) != 0)
AND ((flags_z & 0x10000000) != 0)
/* Not EDGE, NOPROFILE, PEAKCENTER, NOTCHECKED
PSF_FLUX_INTERP, SATURATED, or BAD_COUNTS_ERROR */
AND ((flags_i & 0x8100000c00a4) = 0)
AND ((flags_z & 0x8100000c00a4) = 0)
/* Not DEBLEND_NOPEAK or small PSF error */
AND (((flags_i & 0x400000000000) = 0) or (psfmagerr_i <= 0.2))
AND (((flags_z & 0x400000000000) = 0) or (psfmagerr_z <= 0.2))
/* Not INTERP_CENTER or not COSMIC_RAY */
AND (((flags_i & 0x100000000000) = 0) or (flags_i & 0x1000) = 0)
AND (((flags_z & 0x100000000000) = 0) or (flags_z & 0x1000) = 0)
```

```
AND distanceMins IN (
SELECT MIN(distanceMins) FROM gcsSourceXDR7PhotoObj WHERE
masterObjID = x.masterObjID AND distanceMins < 1.0 / 60
```

```
)
)
```

```
AS T2 RIGHT OUTER JOIN gcsSource AS g on g.sourceID=T2.masterObjID
WHERE
```

```
/* Sample selection predicates: Praesepe RA=120-150 deg && dec=15-25 deg */
g.ra BETWEEN 120.0 AND 135.0
AND g.dec BETWEEN 15.0 AND 25.0 and
(zXi BETWEEN -1.0 AND +1.0 OR zXi < -0.9e9)
AND yXi BETWEEN -1.0 AND +1.0
AND jXi BETWEEN -1.0 AND +1.0
AND hXi BETWEEN -1.0 AND +1.0
AND k_1Xi BETWEEN -1.0 AND +1.0
AND (zEta BETWEEN -1.0 AND +1.0 OR zEta < -0.9e9)
AND yEta BETWEEN -1.0 AND +1.0
AND jEta BETWEEN -1.0 AND +1.0
AND hEta BETWEEN -1.0 AND +1.0
AND k_1Eta BETWEEN -1.0 AND +1.0
AND (zClass BETWEEN -2 AND -1 OR zClass < -9999)
AND yClass BETWEEN -2 AND -1
AND jClass BETWEEN -2 AND -1
AND hClass BETWEEN -2 AND -1
AND k_1Class BETWEEN -2 AND -1
AND (priOrSec = 0 OR priOrSec = g.frameSetID)
AND g.frameSetID = ml.frameSetID
AND ml.zmflID = m.multiframeID
AND g.zppErrBits < 16
AND g.yppErrBits < 16
AND g.jppErrBits < 16
AND g.hppErrBits < 16
AND g.k_1ppErrBits < 16
AND g.framesetID=f.framesetID
AND f.multiframeID=m.multiframeID
```

A2 UKIDSS-2MASS

```

SELECT
g.sourceID as u_id,
T2.pts_key as t_id,
T2.designation t_designation,
g.ra as u_ra,
g.dec as u_dec,
T2.ra as t_ra,
T2.dec as t_dec,
m.mjdObs as u_mjd,
(T2.jdate-2400000.5) as t_mjd,
g.mergedClass as u_class,
g.zaperMag3 as u_z,
g.zaperMag3Err as u_zerr,
g.yaperMag3 as u_y,
g.yaperMag3Err as u_yerr,
g.japerMag3 as u_j,
g.japerMag3Err as u_jerr,
g.haperMag3 as u_h,
g.haperMag3Err as u_herr,
g.k_laperMag3 as u_k,
g.k_laperMag3Err as u_kerr,
T2.j_m as t_j,
T2.h_m as t_h,
T2.k_m as t_k,
T2.ph_qual as t_phqual,
T2.nopt_mchs as nopt_mchs,

(T2.distanceMins * 60) as ut_separation,

3.6e6*COS(RADIANS(g.dec))*(g.ra-T2.ra)/((m.mjdObs-(T2.jdate-2400000.5))/365.25) AS ut_pmra,
3.6e6*(g.dec-T2.dec)/((m.mjdObs-(T2.jdate-2400000.5))/365.25) AS ut_pmdec,

g.framesetid as framesetid,
f.multiframeid as multiframeid,
m.filename as filename,
m.catname as catname,
f.extNum as extnum

FROM
gcsMergeLog AS ml,
Multiframe AS m,
gcsFrameSets as f,

(
  SELECT mass.designation, mass.pts_key, mass.ra, mass.dec, x.slaveObjID, x.masterObjID,
  x.distanceMins, mass.j_m, mass.h_m, mass.k_m,
  mass.ph_qual, mass.nopt_mchs

  FROM gcsSourceXtwomass_psc AS x, TWOMASS..twomass_psc as mass

  WHERE x.slaveObjID = mass.pts_key AND mass.j_m > 9 AND mass.h_m > 8.5 AND mass.k_m > 8 AND
  distanceMins IN(
  SELECT MIN(distanceMins) FROM gcsSourceXtwomass_psc WHERE
  masterObjID = x.masterObjID AND distanceMins < 1.0 / 60
)
)
AS T2 RIGHT OUTER JOIN gcsSource AS g on g.sourceID=T2.masterObjID
WHERE
/* Sample selection predicates: Praesepe RA=120-135 deg && dec=15-25 deg */
g.ra BETWEEN 120.0 AND 135.0

```

```

AND g.dec BETWEEN 15.0 AND 25.0 and
(zXi BETWEEN -1.0 AND +1.0 OR zXi < -0.9e9)
AND yXi BETWEEN -1.0 AND +1.0
AND jXi BETWEEN -1.0 AND +1.0
AND hXi BETWEEN -1.0 AND +1.0
AND k_1Xi BETWEEN -1.0 AND +1.0
AND (zEta BETWEEN -1.0 AND +1.0 OR zEta < -0.9e9)
AND yEta BETWEEN -1.0 AND +1.0
AND jEta BETWEEN -1.0 AND +1.0
AND hEta BETWEEN -1.0 AND +1.0
AND k_1Eta BETWEEN -1.0 AND +1.0
AND (zClass BETWEEN -2 AND -1 OR zClass < -9999)
AND yClass BETWEEN -2 AND -1
AND jClass BETWEEN -2 AND -1
AND hClass BETWEEN -2 AND -1
AND k_1Class BETWEEN -2 AND -1
AND (priOrSec = 0 OR priOrSec = g.frameSetID)
AND g.frameSetID = ml.frameSetID
AND ml.zmflID = m.multiframeID
AND g.zppErrBits < 16
AND g.yppErrBits < 16
AND g.jppErrBits < 16
AND g.hppErrBits < 16
AND g.k_1ppErrBits < 16
AND g.framesetID=f.framesetID
AND f.multiframeID=m.multiframeID

```

APPENDIX B: HIGH PROBABILITY MEMBERS MATCHED TO PREVIOUS WORKS

7

Table B1: High Probability Members Matched to Previous Works

ID	Z	Y	J	H	K	μ_α (mas yr ⁻¹)	μ_δ	Pmem (%)	Previous IDs
UGCSJ083545.87+223042.	14.70	14.27	13.75	13.18	12.89	-35.9	-11.8	0.65	AD2057; KH561
UGCSJ084207.83+221105.	14.84	14.39	13.84	13.27	12.99	-35.5	-7.3	0.76	AD3054; HSHJ406; KH691
UGCSJ083722.41+220200.	14.11	13.61	13.05	12.52	12.21	-34.0	-4.2	0.77	AD2305; KH799
UGCSJ084440.47+214553.	14.08	13.71	13.20	12.62	12.32	-34.6	-1.3	0.71	AD3337; KH508
UGCSJ084120.88+215453.	13.96	13.71	13.24	12.64	12.43	-28.5	-10.4	0.75	AD2939
UGCSJ084302.88+214513.	15.13	14.57	13.97	13.44	13.08	-29.6	-9.6	0.73	AD3161; KH989
UGCSJ083256.66+213829.	15.82	15.43	14.92	14.36	14.05	-38.2	-6.3	0.69	AD1687
UGCSJ084126.00+213425.	15.93	15.42	14.82	14.31	13.94	-36.7	-3.8	0.72	AD2951; HSHJ367; KH901
UGCSJ084458.84+213217.	15.64	15.28	14.76	14.28	13.98	-27.8	-0.6	0.61	AD3361
UGCSJ083454.93+213854.	15.19	14.75	14.17	13.59	13.28	-34.2	-1.4	0.71	AD1951; KH773
UGCSJ083526.81+213901.	15.74	15.25	14.65	14.10	13.77	-37.8	-8.8	0.68	AD2021; KH843
UGCSJ083912.55+213557.	15.90	15.43	14.81	14.24	13.93	-29.2	-7.2	0.75	AD2517; HSHJ250
UGCSJ083413.87+212352.	15.25	14.75	14.18	13.61	13.31	-27.8	-8.1	0.71	AD1868; KH786
UGCSJ083434.27+212207.	14.54	14.06	13.46	12.89	12.59	-29.2	-5.2	0.75	AD1915; KH681
UGCSJ083316.62+212020.	14.08	13.64	13.11	12.54	12.26	-29.8	-9.3	0.74	AD1737; KH677
UGCSJ084143.40+212950.	15.93	15.25	14.60	14.08	13.70	-31.7	-12.4	0.67	AD3006; HSHJ386; KH1084
UGCSJ084030.70+212333.	14.94	14.56	14.04	13.47	13.19	-29.1	-9.0	0.73	AD2776; HSHJ318;
UGCSJ084048.51+212949.	13.64	13.43	13.00	12.40	12.24	-26.0	-8.8	0.81	AD2828
UGCSJ082935.64+212047.	14.79	14.53	14.07	13.45	13.26	-31.2	-4.2	0.77	AD1252
UGCSJ084536.22+211521.	13.74	13.38	12.87	12.28	12.01	-26.8	-1.4	0.73	AD3427; HSHJ497; JS604; KH450
UGCSJ084457.00+210648.	15.58	15.11	14.54	13.97	13.67	-28.3	-6.2	0.73	AD3358; KH835
UGCSJ083813.89+210926.	13.91	13.55	13.07	12.47	12.21	-31.8	-9.9	0.63	HSHJ198; JS216; KH453
UGCSJ083459.25+210837.	15.42	14.84	14.24	13.69	13.37	-32.9	-1.7	0.73	AD1962; KH961
UGCSJ084123.94+211519.	15.62	15.24	14.73	14.17	13.90	-28.4	-3.9	0.72	AD2945
UGCSJ084719.06+211102.	15.58	15.11	14.51	13.95	13.64	-25.2	-6.3	0.60	KH814
UGCSJ084711.92+210748.	15.72	15.22	14.60	14.07	13.74	-32.4	-12.3	0.67	HSHJ501; KH926
UGCSJ083730.73+210740.	14.94	14.51	13.99	13.42	13.13	-32.7	-9.7	0.75	KH564
UGCSJ082927.94+210838.	13.39	13.11	12.65	12.04	11.80	-31.1	-3.6	0.78	AD1240; KH397
UGCSJ084515.55+210335.	14.41	14.04	13.52	12.96	12.69	-36.0	-1.9	0.70	AD3394; HSHJ496; KH574
UGCSJ084620.04+210032.	15.80	15.29	14.69	14.14	13.82	-36.7	-6.4	0.73	AD3506; HSHJ499; KH927
UGCSJ084321.75+205510.	15.07	14.78	14.28	13.74	13.48	-26.7	-4.8	0.67	AD3195
UGCSJ082942.64+205707.	14.03	13.78	13.28	12.70	12.48	-28.4	-0.3	0.61	AD1263
UGCSJ083629.41+210310.	14.94	14.54	14.01	13.44	13.16	-31.7	-13.5	0.61	AD2175; HSHJ125; KH614
UGCSJ083715.24+205759.	14.20	13.90	13.42	12.82	12.59	-27.5	-2.5	0.66	AD2291
UGCSJ083401.54+210039.	15.77	15.27	14.67	14.11	13.80	-25.4	-5.6	0.61	AD1837; KH871
UGCSJ084114.43+205946.	15.63	15.17	14.58	14.02	13.71	-30.7	-1.0	0.70	AD2918; HSHJ356; KH838
UGCSJ084859.88+204155.	15.69	15.12	14.50	13.99	13.62	-39.3	-6.6	0.63	KH965
UGCSJ083918.03+204421.	13.67	13.36	12.86	12.26	12.05	-31.6	-8.5	0.74	AD2538; JS284; KH419
UGCSJ083922.13+204758.	15.27	14.78	14.20	13.65	13.32	-32.3	-4.5	0.78	AD2551; HSHJ261; KH828
UGCSJ083232.42+205040.	14.45	14.06	13.53	12.95	12.70	-26.5	-5.8	0.67	AD1632; JS10; KH528
UGCSJ083845.67+203943.	15.44	15.02	14.43	13.90	13.60	-34.5	-4.1	0.77	AD2452; KH812
UGCSJ083615.51+204109.	13.15	12.90	12.44	11.83	11.62	-31.7	-4.8	0.78	AD2138; JS117; KH357
UGCSJ083603.23+205015.	15.67	15.18	14.61	14.08	13.74	-33.6	-5.7	0.78	AD2101; HSHJ096; KH841
UGCSJ084114.04+204429.	13.97	13.53	12.96	12.38	12.12	-26.5	-5.2	0.87	AD2916; JS416; KH707
UGCSJ083711.87+204047.	14.03	13.72	13.20	12.59	12.35	-27.7	-11.9	0.61	AD2284; JS1661; KH477
UGCSJ083406.67+204946.	15.71	15.26	14.68	14.11	13.80	-29.4	-5.6	0.76	AD1852; KH818
UGCSJ084418.23+204948.	15.45	14.94	14.32	13.76	13.46	-38.4	-1.7	0.61	AD3300; HSHJ478
UGCSJ083300.38+204310.	13.72	13.35	12.79	12.23	11.95	-32.0	-3.9	0.73	AD1699; JS19; KH706
UGCSJ083804.60+203935.	14.95	14.53	13.95	13.38	13.08	-33.0	-10.4	0.74	KH663; JS704;
UGCSJ084849.96+202635.	13.44	13.15	12.66	12.07	11.81	-28.7	-4.3	0.86	KH392
UGCSJ085032.50+203419.	14.27	13.97	13.51	12.99	12.81	-34.0	-0.3	0.68	AD3783
UGCSJ084545.87+202940.	13.78	13.44	12.92	12.34	12.09	-28.4	-8.8	0.83	AD3447; JS609; KH460
UGCSJ084047.77+202847.	14.03	13.61	13.09	12.49	12.25	-33.6	-7.9	0.78	AD2825; KH554
UGCSJ083314.23+203621.	15.71	15.20	14.57	14.03	13.72	-28.5	-8.4	0.72	AD1731; KH892
UGCSJ083808.16+202646.	13.70	13.35	12.82	12.22	12.01	-30.8	-6.5	0.83	KH418
UGCSJ084611.69+203800.	14.36	14.04	13.50	12.99	12.71	-32.2	-6.8	0.79	AD3490
UGCSJ083338.36+202852.	15.31	14.82	14.25	13.71	13.43	-27.1	-10.7	0.62	AD1786; KH724
UGCSJ083943.59+202939.	14.54	14.14	13.60	13.03	12.75	-25.7	-5.7	0.63	AD2618; JS311; KH629
UGCSJ083912.08+203607.	14.84	14.38	13.82	13.27	12.96	-39.3	-6.0	0.64	AD2515
UGCSJ083903.93+203402.	13.98	13.60	13.07	12.50	12.24	-25.8	-7.4	0.84	AD2502; JS266; KH500
UGCSJ082750.59+201436.	12.50	12.26	11.85	11.32	11.09	-26.0	-0.4	0.60	AD1025; KH300
UGCSJ084111.05+202238.	13.44	13.12	12.63	12.04	11.81	-25.7	-5.8	0.85	AD2905; JS411; KH416
UGCSJ084137.35+201236.	15.15	14.66	14.09	13.56	13.27	-30.2	-1.2	0.69	AD2988; HSHJ381; KH667
UGCSJ083641.16+201639.	15.04	14.60	13.98	13.45	13.14	-30.7	-5.6	0.78	AD2205; KH693
UGCSJ083642.16+201622.	15.46	14.97	14.37	13.85	13.52	-32.3	-9.9	0.75	AD2208
UGCSJ084423.19+201355.	15.34	14.84	14.28	13.72	13.42	-29.1	-4.8	0.75	AD3312; KH787
UGCSJ083041.51+202426.	15.55	15.17	14.68	14.10	13.84	-37.2	-9.0	0.69	AD1396
UGCSJ083311.09+201604.	15.16	14.74	14.17	13.67	13.37	-31.8	-12.6	0.66	AD1719
UGCSJ083942.01+201745.	14.98	14.50	13.93	13.39	13.11	-31.5	-0.8	0.70	AD2615; KH808
UGCSJ083906.87+202054.	13.54	13.23	12.75	12.14	11.94	-25.1	-5.5	0.83	AD2508; JS270; KH426
UGCSJ083507.87+202023.	14.46	14.07	13.55	12.99	12.71	-30.9	-9.5	0.75	AD1978; KH496

Continued on next page

7 AD = Adams et al. (2002), HSHJ = Hambly et al. (1995b), JS = Jones & Cudworth (1983) and KH = Kraus & Hillenbrand (2007),.

Table B1– continued from previous page

ID	Z	Y	J	H	K	μ_α (mas yr ⁻¹)	μ_δ	Pmem (%)	Previous IDs
UGCSJ083436.75+201155.	13.71	13.41	12.93	12.32	12.08	-30.4	-6.4	0.84	AD1921; HSHJ058; JS63
UGCSJ084151.90+202047.	13.85	13.51	13.00	12.41	12.18	-29.9	-8.4	0.82	AD3026; JS459; KH470
UGCSJ083855.15+201308.	14.31	13.90	13.35	12.77	12.50	-32.3	0.1	0.67	AD2478; HSHJ234; JS255; KH606
UGCSJ083825.35+202120.	15.93	15.45	14.85	14.32	13.99	-31.1	-11.8	0.69	KH903
UGCSJ083539.26+202409.	14.98	14.48	13.88	13.35	13.04	-31.4	-8.2	0.77	AD2042; KH854
UGCSJ085237.29+200043.	13.46	13.26	12.84	12.27	12.13	-26.4	-5.0	0.86	AD4003
UGCSJ083259.56+200714.	15.87	15.39	14.81	14.27	13.93	-33.9	-12.6	0.65	AD1696; KH896
UGCSJ084332.60+195932.	14.73	14.31	13.75	13.19	12.88	-34.2	-3.9	0.77	AD3211; HSHJ458; KH655
UGCSJ083333.93+200425.	14.27	13.89	13.36	12.76	12.52	-26.6	-6.4	0.67	AD1774; HSHJ043; KH509
UGCSJ083559.43+200440.	14.87	14.41	13.81	13.26	12.95	-36.5	-1.0	0.66	AD2091; HSHJ091; JS687; KH743
UGCSJ083622.40+200706.	15.36	14.89	14.32	13.76	13.45	-26.3	-7.9	0.65	AD2155; KH774
UGCSJ084034.83+194937.	14.85	14.52	14.04	13.46	13.19	-34.7	-5.9	0.77	AD2790
UGCSJ083608.58+195725.	15.13	14.65	14.05	13.49	13.19	-26.1	-9.0	0.62	AD2115; HSHJ102; KH884
UGCSJ083619.14+195354.	14.34	13.94	13.41	12.82	12.56	-31.4	-8.2	0.77	AD2147; HSHJ115; JS123; KH593
UGCSJ083707.63+195727.	15.47	14.99	14.43	13.87	13.56	-32.5	-7.8	0.78	AD2275; KH864
UGCSJ083727.87+195412.	14.32	13.91	13.38	12.78	12.53	-32.7	-11.3	0.71	AD2328; KH638
UGCSJ084030.57+195558.	14.15	13.76	13.25	12.64	12.42	-27.0	-10.5	0.63	AD2775; HSHJ320; JS356; KH546
UGCSJ084801.27+194939.	15.40	14.95	14.37	13.79	13.50	-32.5	-5.6	0.79	KH727
UGCSJ084823.56+195011.	14.64	14.23	13.65	13.07	12.78	-31.9	1.1	0.62	KH579
UGCSJ085056.86+193657.	14.44	14.05	13.52	12.93	12.67	-30.7	0.6	0.63	KH527
UGCSJ082757.39+191130.	15.94	15.55	14.98	14.37	14.12	-36.2	-9.1	0.72	AD1043
UGCSJ083439.68+190812.	14.61	14.18	13.63	13.05	12.78	-32.7	-4.5	0.78	AD1925; HSHJ060; KH596
UGCSJ083430.71+190600.	14.46	14.08	13.53	12.96	12.73	-38.2	-9.9	0.63	AD1906; HSHJ055; JS675; KH513
UGCSJ082848.63+185835.	15.82	15.26	14.63	14.07	13.72	-31.5	-5.9	0.78	AD1164; KH1025
UGCSJ083150.86+185902.	15.29	14.85	14.32	13.79	13.47	-29.9	0.6	0.62	AD1549
UGCSJ083218.87+190308.	14.64	14.21	13.64	13.08	12.78	-33.6	-8.4	0.77	AD1607; HSHJ023; KH594
UGCSJ083544.59+185738.	15.40	14.93	14.35	13.80	13.50	-29.2	-6.0	0.75	AD2053; HSHJ084; KH858
UGCSJ083651.05+190418.	14.99	14.61	14.09	13.51	13.22	-28.7	-4.4	0.73	AD2231; HSHJ136; KH565
UGCSJ083305.56+185548.	13.93	13.55	13.01	12.43	12.17	-22.8	-4.3	0.66	AD1707; JS22; KH519
UGCSJ083338.00+185717.	14.21	13.86	13.31	12.74	12.49	-38.5	-7.4	0.67	AD1785; HSHJ045; JS41; KH482
UGCSJ083051.38+185351.	15.25	14.81	14.22	13.66	13.38	-32.3	0.0	0.67	AD1411; HSHJ008; KH670
UGCSJ083734.95+185607.	14.47	14.11	13.60	13.09	12.84	-32.2	-6.9	0.79	HSHJ173
UGCSJ083235.23+184409.	15.94	15.41	14.79	14.24	13.95	-27.6	-6.1	0.71	AD1641; HSHJ024
UGCSJ083207.94+184426.	14.37	13.97	13.47	12.87	12.59	-26.9	-1.6	0.61	AD1588; KH511
UGCSJ083154.25+184536.	15.59	15.08	14.51	13.96	13.64	-28.9	-5.9	0.75	AD1555; HSHJ018; KH834
UGCSJ083126.88+184056.	15.41	14.84	14.19	13.64	13.30	-29.9	-6.8	0.77	AD1500; KH1044
UGCSJ083658.63+184952.	15.19	14.63	14.04	13.51	13.17	-28.2	-7.6	0.72	AD2248; KH923
UGCSJ083808.07+184429.	15.80	15.28	14.68	14.11	13.82	-27.0	-10.5	0.63	HSHJ196; KH779
UGCSJ083729.39+184135.	14.89	14.48	13.94	13.38	13.10	-37.7	-7.2	0.70	HSHJ165; KH542
UGCSJ083528.37+184032.	15.73	15.21	14.63	14.10	13.76	-27.3	-3.6	0.68	AD2022
UGCSJ083506.21+184924.	14.76	14.33	13.77	13.20	12.92	-38.7	-3.8	0.64	AD1975; HSHJ068; JS680; KH644
UGCSJ083540.13+184228.	14.15	13.72	13.18	12.62	12.33	-34.2	-5.9	0.78	AD2045; HSHJ082; JS95; KH636
UGCSJ083434.30+184756.	14.13	13.73	13.19	12.62	12.37	-32.5	-12.6	0.66	AD1917; HSHJ056; JS62; KH570
UGCSJ083343.93+184750.	14.31	13.90	13.40	12.81	12.54	-31.9	-13.7	0.60	AD1797; HSHJ047; JS44; KH526
UGCSJ083328.19+184336.	15.96	15.40	14.81	14.28	13.95	-38.4	-4.3	0.67	AD1763; HSHJ041; KH874
UGCSJ083142.95+182906.	15.26	14.81	14.22	13.64	13.36	-26.2	-7.9	0.65	AD1532; HSHJ017; KH699
UGCSJ083140.88+182942.	14.89	14.47	13.90	13.34	13.08	-32.9	-5.7	0.79	AD1526; HSHJ016; KH563
UGCSJ083521.67+182934.	13.98	13.59	13.11	12.53	12.28	-27.0	-7.6	0.86	AD2011; HSHJ076; JS87; KH463
UGCSJ083334.78+183108.	13.24	12.97	12.54	11.98	11.84	-26.6	-3.3	0.83	AD1776; JS40
UGCSJ083014.08+182519.	14.56	14.15	13.61	13.08	12.78	-35.1	-11.9	0.66	AD1344; HSHJ004; KH559
UGCSJ083453.83+180105.	15.72	15.23	14.61	14.05	13.73	-32.0	-10.9	0.72	AD1948; HSHJ065; KH817
UGCSJ083547.20+180829.	14.54	14.12	13.52	12.94	12.67	-30.7	-11.7	0.69	AD2063; HSHJ087; KH628
UGCSJ083002.92+175702.	15.79	15.24	14.65	14.07	13.72	-32.0	-12.0	0.69	AD1308; HSHJ002; KH990
UGCSJ083517.03+173624.	15.12	14.59	14.00	13.43	13.14	-27.1	-7.7	0.68	AD2000; HSHJ074; KH855
UGCSJ083839.13+172948.	15.98	15.49	14.88	14.33	14.02	-30.6	-10.7	0.72	AD2436; HSHJ217; KH904
UGCSJ084026.64+172100.	14.82	14.48	13.98	13.40	13.13	-29.9	-2.9	0.73	AD2760
UGCSJ083855.64+171509.	14.51	14.12	13.56	12.99	12.70	-27.4	-2.3	0.65	AD2482; KH608
UGCSJ083824.87+165836.	14.09	13.71	13.16	12.59	12.31	-32.8	-2.0	0.74	AD2396; KH478
UGCSJ083906.50+170100.	14.58	14.06	13.51	12.96	12.64	-36.2	-7.5	0.74	AD2507
UGCSJ083608.51+165717.	13.88	13.54	13.05	12.50	12.22	-29.8	-4.0	0.84	AD2114

APPENDIX C: NEW HIGH PROBABILITY MEMBERS

Table C1: New High Probability Members

ID	<i>Z</i>	<i>Y</i>	<i>J</i>	<i>H</i>	<i>K</i>	μ_α (mas yr ⁻¹)	μ_δ (mas yr ⁻¹)	Pmem
UGCSJ083925.46+214721.9	15.46	15.12	14.62	14.06	13.81	-31.1	-8.8	0.76
UGCSJ083301.71+213902.1	13.95	13.75	13.35	12.73	12.58	-24.6	-4.5	0.80
UGCSJ084826.25+213235.7	15.98	15.59	15.02	14.48	14.20	-32.4	-1.6	0.73
UGCSJ083310.88+210959.8	13.38	13.15	12.71	12.10	11.92	-22.9	-6.5	0.70
UGCSJ083032.17+211015.4	15.26	14.96	14.46	13.84	13.66	-29.4	-7.3	0.76
UGCSJ083956.01+211419.1	15.84	15.49	15.00	14.43	14.18	-25.5	-4.8	0.61
UGCSJ083553.75+191055.8	15.11	14.85	14.39	13.79	13.61	-26.2	-6.3	0.65
UGCSJ083115.62+184708.9	15.89	15.58	15.13	14.57	14.35	-31.1	-0.3	0.68
UGCSJ083448.26+181300.2	14.46	14.26	13.82	13.21	13.08	-27.6	-4.5	0.70
UGCSJ083459.25+181805.4	15.43	15.19	14.71	14.10	13.88	-32.9	-1.5	0.72
UGCSJ083306.96+174242.1	15.29	14.77	14.16	13.61	13.31	-26.3	-3.6	0.63
UGCSJ083701.06+172005.1	14.80	14.47	13.94	13.41	13.12	-28.1	-7.2	0.72
UGCSJ084709.34+172925.6	15.45	15.11	14.58	14.12	13.87	-33.1	-9.3	0.76
UGCSJ083455.71+170918.5	13.90	13.72	13.30	12.70	12.56	-22.6	-4.1	0.63

APPENDIX D: SDSS CANDIDATE MEMBERS

8

Table D1: SDSS-UKIDSS selected candidates

ID	<i>Z</i>	<i>Y</i>	<i>J</i>	<i>H</i>	<i>K</i>	μ_α	μ_δ	Prob	Fit Order
						(mas yr ⁻¹)			
UGCSJ084218.27+212342.1	18.18	17.50	16.81	16.27	15.88	-4.05	-6.32	0.00	12
UGCSJ084804.97+211515.1	19.64	18.57	17.68	17.05	16.59	67.66	64.70	0.00	6
UGCSJ084346.46+210829.4	18.46	17.68	17.00	16.45	16.06	-28.38	-38.64	0.00	12
UGCSJ084956.26+205300.0	17.88	17.30	16.65	16.09	15.71	32.59	-53.01	0.00	12
UGCSJ082924.86+211700.3	16.10	15.59	15.02	14.57	14.27	-94.95	-133.65	0.00	12
UGCSJ084138.84+211655.5	17.88	17.29	16.55	16.03	15.72	9.02	20.03	0.00	12
UGCSJ084449.14+210153.6	18.77	17.79	16.95	16.41	15.94	0.36	23.91	0.00	12
UGCSJ084507.41+210056.5	18.69	17.87	17.06	16.49	16.14	-36.74	-40.16	0.00	12
UGCSJ084204.64+205941.1	16.77	16.09	15.42	14.93	14.54	114.67	-167.13	0.00	12
UGCSJ082839.58+205401.5	18.48	17.69	16.91	16.34	15.95	15.24	-31.20	0.00	12
UGCSJ082945.32+205455.0	19.26	18.48	17.67	17.10	16.51	4.16	-22.41	0.00	12
UGCSJ083054.47+190119.4	16.13	15.47	14.76	14.21	13.84	-15.32	-128.89	0.00	12
UGCSJ084433.77+214430.7	17.77	17.01	16.30	15.74	15.32	-37.33	32.77	0.00	6
UGCSJ084650.44+214805.4	17.37	16.68	16.08	15.62	15.28	-75.34	-117.60	0.00	12
UGCSJ083301.71+213534.7	18.65	17.93	17.20	16.61	16.17	14.87	18.57	0.00	6
UGCSJ084306.24+214134.2	18.40	17.56	16.71	16.16	15.73	-38.63	-44.50	0.00	12
UGCSJ083141.80+183500.4	15.65	15.07	14.45	13.98	13.64	46.31	-110.20	0.00	12
UGCSJ083353.37+182609.4	19.20	18.17	17.24	16.64	16.18	6.73	-8.95	0.00	12
UGCSJ083955.10+222300.8	19.06	18.11	17.27	16.64	16.21	-11.29	-9.27	0.58	12
UGCSJ083110.12+181252.7	18.15	17.48	16.74	16.20	15.75	38.81	-45.95	0.00	12
UGCSJ083654.60+195415.7	18.75	17.96	17.10	16.53	15.96	-26.97	28.33	0.00	12
UGCSJ083648.03+194902.2	18.21	17.34	16.55	15.97	15.52	-98.98	-17.63	0.00	6
UGCSJ084714.47+194643.8	18.06	17.45	16.80	16.27	15.86	14.68	6.35	0.00	12
UGCSJ085052.56+195321.9	19.24	18.34	17.40	16.75	16.22	-5.74	-21.30	0.00	12
UGCSJ084652.65+172017.9	18.67	17.91	17.15	16.62	16.18	16.12	-30.63	0.00	12
UGCSJ084045.71+171218.3	19.09	18.17	17.20	16.60	16.17	-33.60	1.04	0.58	12
UGCSJ084452.78+171409.8	18.77	17.76	16.90	16.33	15.84	-44.67	-13.78	0.00	12
UGCSJ083900.61+204356.2	20.05	18.76	17.91	17.33	16.72	2.62	-71.34	0.00	12
UGCSJ083920.28+204629.5	19.34	18.49	17.65	16.95	16.51	-5.94	-12.50	0.00	12
UGCSJ083721.24+204306.1	19.73	18.66	17.56	16.84	16.33	25.55	9.35	0.00	12
UGCSJ083737.24+202902.6	19.71	18.60	17.39	16.64	16.04	-34.02	-61.35	0.00	12
UGCSJ083019.80+203418.8	18.95	17.92	17.11	16.59	16.13	-10.23	-93.17	0.00	12
UGCSJ083724.09+164812.9	18.55	17.81	17.10	16.53	16.10	-5.67	11.58	0.00	12
UGCSJ083954.96+202955.7	18.90	17.91	17.06	16.44	15.98	33.38	-54.56	0.00	12
UGCSJ084926.31+202127.0	18.64	17.76	17.00	16.54	16.08	-75.67	-30.17	0.00	12
UGCSJ085002.02+201725.9	19.28	18.56	17.64	17.05	16.53	-44.04	50.96	0.00	12
UGCSJ083203.66+202035.8	19.90	18.68	17.74	17.04	16.52	-31.90	-59.39	0.00	12
UGCSJ083531.32+201838.9	18.39	17.62	16.96	16.39	15.99	-17.01	20.43	0.00	12
UGCSJ083748.01+201448.5	18.09	17.25	16.51	15.94	15.53	-36.17	-44.57	0.00	12

This paper has been typeset from a \LaTeX file prepared by the author.

⁸ For some objects not enough reference stars could be found to perform the quadratic fit. In this case the fit was reduced to a linear one (6 free parameters) as indicated in the fit order column.